

Fall 2017

Electrical properties of metal semiconductor contacts - metals on MoS₂: a case study

Xiao Chang

New Jersey Institute of Technology

Follow this and additional works at: <https://digitalcommons.njit.edu/theses>



Part of the [Other Physics Commons](#)

Recommended Citation

Chang, Xiao, "Electrical properties of metal semiconductor contacts - metals on MoS₂: a case study" (2017). *Theses*. 43.
<https://digitalcommons.njit.edu/theses/43>

This Thesis is brought to you for free and open access by the Theses and Dissertations at Digital Commons @ NJIT. It has been accepted for inclusion in Theses by an authorized administrator of Digital Commons @ NJIT. For more information, please contact digitalcommons@njit.edu.

Copyright Warning & Restrictions

The copyright law of the United States (Title 17, United States Code) governs the making of photocopies or other reproductions of copyrighted material.

Under certain conditions specified in the law, libraries and archives are authorized to furnish a photocopy or other reproduction. One of these specified conditions is that the photocopy or reproduction is not to be “used for any purpose other than private study, scholarship, or research.” If a user makes a request for, or later uses, a photocopy or reproduction for purposes in excess of “fair use” that user may be liable for copyright infringement,

This institution reserves the right to refuse to accept a copying order if, in its judgment, fulfillment of the order would involve violation of copyright law.

Please Note: The author retains the copyright while the New Jersey Institute of Technology reserves the right to distribute this thesis or dissertation

Printing note: If you do not wish to print this page, then select “Pages from: first page # to: last page #” on the print dialog screen

The Van Houten library has removed some of the personal information and all signatures from the approval page and biographical sketches of theses and dissertations in order to protect the identity of NJIT graduates and faculty.

ABSTRACT

ELECTRICAL PROPERTIES OF METAL SEMICONDUCTOR CONTACTS – METALS ON MoS₂: A CASE STUDY

**by
Xiao Chang**

Properties of monolayer semiconductor, MoS₂, are presented in the research. Schottky barrier height and Schottky-Mott rules are discussed. The current-voltage measurement and capacitance-voltage measurement are analyzed considering the role of the work function. We mainly focus on metal semiconductor contacts on molybdenum disulfide (MoS₂). The properties of bulk and monolayer molybdenum disulfide are discussed. The differences between the bulk and monolayer, based on band gap structure theory, are presented. Utilizing the data obtained in the literature, the influence of temperature on the electrical properties of monolayer molybdenum disulfide are analyzed. In particular, the electrical properties of metals on MoS₂ such as current-voltage (I-V) characteristics and capacitance-voltage (C-V) characteristics are addressed. Applications of metals on MoS₂ are presented.

**ELECTRICAL PROPERTIES OF METAL SEMICONDUCTOR CONTACTS –
METALS ON MoS₂: A CASE STUDY**

**by
Xiao Chang**

**A Thesis
Submitted to the Faculty of
New Jersey Institute of Technology
In Partial Fulfillment of the Requirements for the Degree of
Master of Science in Applied Physics**

Federated Department of Physics

December 2017

Blank Page

APPROVAL PAGE

**ELECTRICAL PROPERTIES OF METAL SEMICONDUCTOR
CONTACTS – METALS ON MoS₂: A CASE STUDY**

Xiao Chang

Dr. N. M. Ravindra, Thesis Advisor Date
Professor of Physics, NJIT

Dr. Michael Jaffe, Committee Member Date
Research Professor of Biomedical Engineering, NJIT

Dr. Keun Hyuk Ahn, Committee Member Date
Associate Professor of Physics, NJIT

Dr. George E. Georgiou, Committee Member Date
Senior University Lecturer of Physics, NJIT

BIOGRAPHICAL SKETCH

Author: Xiao Chang

Degree: Master of Science

Date: December 2017

Undergraduate and Graduate Education:

- Master of Science in Applied Physics,
New Jersey Institute of Technology, Newark, NJ, 2017
- Bachelor of Science in Physics,
University of Science and Technology in China, Hefei, China, 2014

Major: Applied Physics

To my parents, my friends, and my teachers

ACKNOWLEDGEMENT

I would like to express my sincere appreciation to my advisor Dr. N. M. Ravindra for his great support in the last two years. He provided remarkable guidance, valuable resources and gave me support and encouragement throughout the entire research. His patience and motivation helped me when I had difficult problems.

I also want to thank Dr. Michael Jaffe, Dr. Keun Hyuk Ahn and Dr. George E. Georgiou for serving as the committee members for this thesis.

I also want to thank my friends and fellow lab-mates: Yan Liu, Sita Rajyalaxmi Marthi, Asahel Bañobre and Zeel Gandhi. They helped me in various aspects. They provided their advice and ideas that helped me a lot in my research.

Last, but not the least, I would like to express my appreciation to my parents for providing full help and support for the past 25 years.

TABLE OF CONTENTS

Chapter	Page
1 INTRODUCTION.....	1
2 FUNDAMENTALS OF METAL SEMICONDUCTOR CONTACTS.....	3
2.1 Background Knowledge	3
2.2 Metal-semiconductor Contacts	6
2.2.1 Schottky Barrier and Schottky-Mott Model	7
2.2.2 Thermionic Emission Theory	12
3 ANALYSIS OF THE CURRENT-VOLTAGE AND CAPACITANCE-VOLTAGE MEASUREMENTS.....	14
3.1 I-V Measurements.....	14
3.2 C-V Measurements	17
4 PROPERTIES OF MoS ₂	22
4.1 Properties of Bulk MoS ₂	22
4.1.1 Bulk Structure	22
4.2 Electronic Properties of Two-Dimensional MoS ₂	26
4.2.1 Band Structure	26
4.2.2 Temperature's Influence to the Electronic Properties of MoS.....	30
4.3 Optical Properties of Two-Dimensional MoS ₂	33

TABLE OF CONTENTS
(Continued)

Chapter	Page
4.3.1 Raman Spectroscopy	33
4.3.2 Experiment.....	35
4.4 Preparation of Two-Dimensional MoS ₂	37
5 METAL-MoS ₂ CONTACTS.....	40
5.1 Properties	40
5.2 Applications	45
6 FUNCTIONAL FORM OF CURRENT-VOLTAGE CHARACTERISTICS	48
7 CONCLUSION.....	49
APPENDIX.....	51
REFERENCES	64

LISTS OF TABLES

Table		Page
2.1	Schottky Barrier Heights for Electrons on N-Type Silicon (ϕ_{Bn}) and for Holes on p-type Silicon (ϕ_{Bp}).....	10
2.2	Schottky Barrier Heights of Metal Silicide.....	10
2.3	Relationship Between Barrier Heights and Temperature and Voltage.....	11
4.1	Part of the Physical Properties of Bulk MoS ₂	25
4.2	Interband Transitions Near the Gap in Monolayer, Bilayer and Bulk MoS ₂ .	28
4.3	Parameter of 2D MoS ₂	33
5.1	Comparison of Two Different I-V Characteristic Results of Au-MoS ₂ Contact.....	43
5.2	Comparison of Two Different I-V Characteristic Results of Pt-MoS ₂ Contact.....	43
5.3	Performance of different metal/2D MoS ₂ contacts.....	46

LIST OF FIGURES

Figure		Page
2.1	Graphene films.....	4
2.2	Field effect in FLG.....	5
2.3	Reverse recovery waveform for 6H-SiC Schottky barrier diode compared with that for a high-speed silicon P-i-N rectifier.....	7
2.4	Energy band diagram of a M-S contact.....	8
2.5	The graph of the exponential function.....	13
3.1	Transport processes in forward-biased Schottky barrier on n-type semiconductor.....	14
3.2	Potential across the depletion layer at the Schottky junction.....	17
3.3	The plot of $\frac{1}{C^2}$ versus V on the metal-semiconductor contact.....	19
3.4	Small-signal (100 mV and 10 kHz) C-V plot for Graphene/Si contact.....	20
4.1	Three-dimensional schematic representation of a typical MX ₂ structure.....	23
4.2	Crystal unit cell of MoS ₂	24
4.3	Schematics of the structural polytypes.....	24
4.4	Band structure of monolayer, bilayer, and bulk MoS ₂ from QSGW calculation.....	27
4.5	Band map of exfoliated monolayer MoS ₂ along the high symmetry line, Corresponding EDCs (energy distribution curves) and MDCs (momentum distribution curves), band map of exfoliated bilayer, trilayer, bulk MoS ₂	29

LIST OF FIGURES
(Continued)

Figure	Page
4.6 (a-d) 2D curvature intensity plots of the low energy valence band of exfoliated monolayer, bilayer, trilayer, and bulk MoS ₂ , respectively. (e) Thickness dependence of the energy difference between VBM (valence band maximum).....	29
4.7 Energy band gaps as a function of temperature of (a) GaAs, (b) GaP, (c) Si and (d) diamond.....	32
4.8 Energy level diagram in the states involved in Raman spectra.....	34
4.9 Raman active modes in the bulk material and monolayer MoS ₂	35
4.10 Non-resonance room-temperature Raman scattering spectrum from the bulk and monolayer MoS ₂	36
4.11 Room-temperature Raman scattering spectrum from the bulk and monolayer MoS ₂ with the resonant (632.8 nm) excitation	36
4.12 Room-temperature photoluminescence spectra in the bulk material and monolayer MoS ₂ . Measurements were performed with a non-resonant excitation ($\lambda = 532$ nm).....	37
4.13 Schematic of the Anodic Bonding principle.....	38
5.1 Electronic band structure of (top panel) the pristine monolayer and wires and (down panel) the assembled monolayers	40
5.2 The current–voltage (I–V) characteristics of the pristine and assembled monolayers	41
5.3 I-V characteristics for different metal-MoS ₂ contacts.....	42
5.4 Band structure of metal and MoS ₂ for work function > electronic affinity ...	45

LIST OF FIGURES
(Continued)

Figure	Page
A.1 Ag-MoS ₂ current-voltage characteristic curves (a) linear fitting; (b) quadratic fitting; (c) cubic fitting	51
A.2 Au-MoS ₂ current-voltage characteristic curves (a) linear fitting; (b) quadratic fitting; (c) cubic fitting	53
A.3 Cu-MoS ₂ current-voltage characteristic curves (a) linear fitting; (b) quadratic fitting; (c) cubic fitting	54
A.4 Pt-MoS ₂ current-voltage characteristic curves (a) linear fitting; (b) quadratic fitting; (c) cubic fitting	56
A.5 Al-MoS ₂ contact current-voltage characteristic curves (a) linear fitting; (b) quadratic fitting; (c) cubic fitting.....	58
A.6 Au-MoS ₂ contact current-voltage characteristic curves (a) linear fitting; (b) quadratic fitting; (c) cubic fitting	59
A.7 Pt-MoS ₂ contact current-voltage characteristic curves (a) linear fitting; (b) quadratic fitting; (c) cubic fitting	61
A.8 W-MoS ₂ contact current-voltage characteristic curves (a) linear fitting; (b) quadratic fitting; (c) cubic fitting	62

CHAPTER 1

INTRODUCTION

In this Chapter, the structure of the Chapters discussed in this thesis will be given, and a brief overview of the Chapters will be provided.

Chapter 2 is brief review of the Two-Dimensional (2D) semiconductors and metal-semiconductor contacts. The discovery of monolayer carbon films, in the form of graphene, has become an important event in materials science. It has opened the door for scientists to discover various kinds of 2D semiconductors with interesting characteristics. Fundamentals of metal-semiconductor contact are described in this Chapter. These include concepts such as the Schottky barrier height, work function, and factors that influence the characteristics of metal-semiconductor contact. A brief description of the thermionic emission theory is presented.

In Chapter 3, the analysis of electrical properties of metal-2D semiconductor contacts is presented. Data from experiments performed by other scientists and theory introduced in Chapter 2 is quantitative and qualitative analysis of the electrical properties .

Next, in Chapter 4, it will focus on molybdenum disulphide (MoS_2). As a popular material in solid-state physics, MoS_2 has remarkable properties. It is a diamagnetic and indirect bandgap semiconductor. And because of the weak Van der Waals interaction between the atoms, the friction coefficient of MoS_2 is low. So MoS_2 is often used as a

lubricant. This Chapter will introduce the physical and chemical properties of MoS₂, and the 2D monolayer of MoS₂.

In Chapter 5, metal-MoS₂ contacts are discussed. In many applications, metal-MoS₂ contacts are widely used. Some specific examples will be described.

Recent studies on metal-semiconductor contacts will be introduced, including the methods of modeling, some important results and conclusions that have been presented in the past few years.

CHAPTER 2

FUNDAMENTALS OF METAL SEMICONDUCTOR CONTACTS

Two-dimensional (2D) materials have developed quickly during the past few decades since the discovery of their interesting physical properties. They exhibit different optical, electronic, thermal characteristics compared to bulk/3D semiconductor [1-8].

2.1 Background Knowledge

In 2004, Novoselov, Geim and other scientists discovered graphene, a monolayer of carbon [9]. The thickness of multi-layer graphene film only equals several atoms (Figure 2.1). Scientist have found that the properties of this kind of material can be controlled by electric field.

Some measurements have been performed on few-layer graphene (FLG). The resistivity ρ has typical dependence on gate voltage V_g (Figure 2.2). In this figure, it can be seen that the resistivity has a sharp peak at the certain V_g . At the same V_g , the Hall coefficient R_H reverses its sign; it is like the ambipolar field effect in semiconductors. However, there is no zero-conductance region with the Fermi level being pinned inside the band gap [9].

Scientists have explained it by a model of a 2D metal with a small overlap between valence and conduction bands.

Scientists have found that 2D crystals exhibit high crystal quality [9, 10]. In the latter, the charge carriers can travel a significant amount of interatomic distance without scattering.

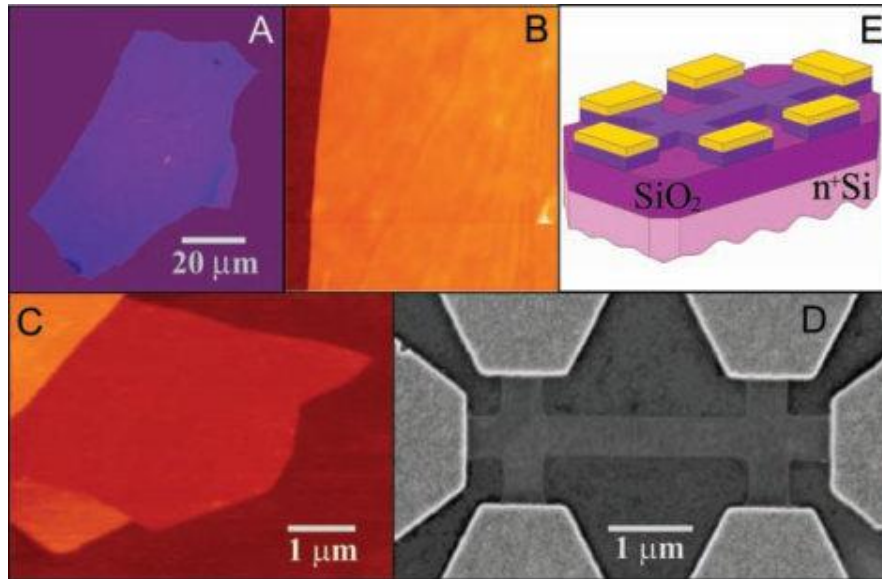


Figure 2.1 Graphene Films - (A) Photograph of a relatively large multilayer graphene flake with thickness ~ 3 nm on top of an oxidized Si wafer. (B) Atomic force microscope (AFM) image of this flake near its edge. Colors: dark brown, SiO₂ surface; orange, 3 nm height above the SiO₂ surface. (C) AFM image of single-layer graphene. (D) Scanning electron microscope image of one of the experimental devices prepared from few-layer graphene. (E) Schematic view of the device in (D).

Source: Novoselov, K.S., et al., Electric field effect in atomically thin carbon films. *Science*, 2004. **306**(5696): p. 666-9.

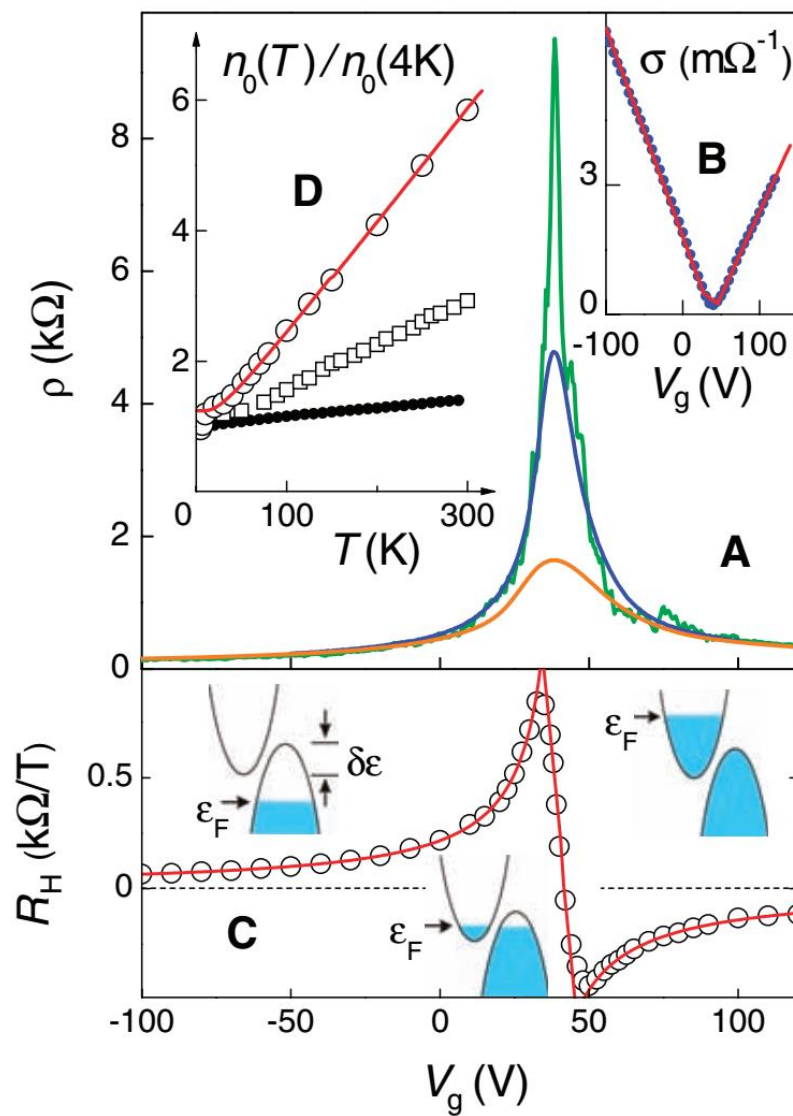


Figure 2.2 Field effect in few-layer graphene. The relationship between the gate voltage and the resistivity at various temperatures.

Source: Novoselov, K.S., et al., Electric field effect in atomically thin carbon films. *Science*, 2004. **306**(5696): p. 666-9.

2.2 Metal-semiconductor Contacts

In solid-state physics, the metal-semiconductor contact (M-S contact) is a kind of contact that has a close contact with the metal and semiconductor. There are two kinds of M-S contacts. The contact between metal and lightly doped semiconductor is called Schottky diode, and the contact between deeply doped semiconductor and metal is called Ohmic contact.

Schottky diode is a rectifying M-S contact, that the model of which was suggested by Walter H. Schottky in 1938. To honor his contribution, the device was named Schottky diode.

The Schottky diode has lower forward voltage drop (0.15~0.45 V) compared to the regular diode (0.7~1.7 V). Because of this characteristic, the Schottky diode can switch very fast to improve the efficiency of electrical equipment. The reverse recovery time is shorter than a regular P-i-N diode (Figure 2.3).

The Ohmic contact is a non-rectifying contact; it has a linear current-voltage characteristic that obeys Ohm's law.

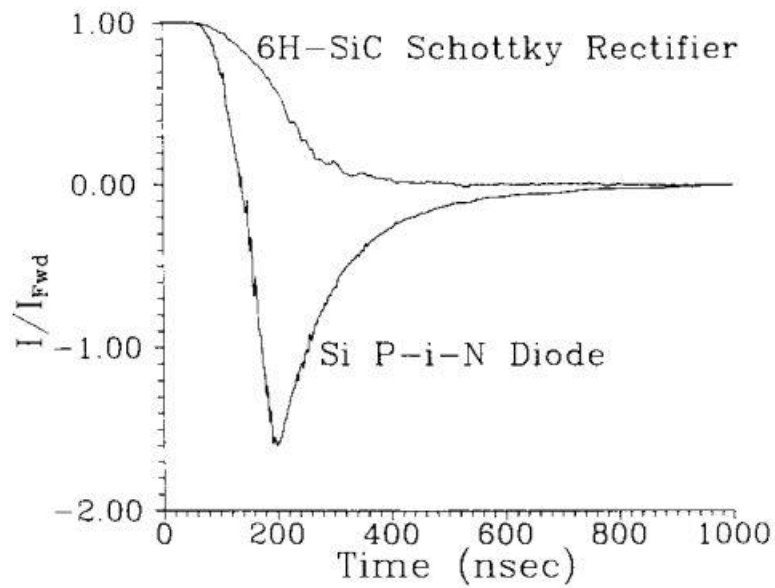


Figure 2.3 Reverse recovery waveform for 6H-SiC Schottky barrier diode compared with that of a high-speed silicon P-i-N rectifier.

Source: Bhatnagar, M., P.K. McLarty, and B.J. Baliga, Silicon-carbide high-voltage (400 V) Schottky barrier diodes. IEEE Electron Device Letters, 1992. **13**(10): p. 501-503.

2.2.1 Schottky Barrier and Schottky-Mott Model

One of the important parameters of M-S contacts is Schottky barrier. It is the potential energy barrier of the electron when a contact is formed between metal and semiconductor.

As shown in Figure 2.4, at the right end of the junction, the energy band diagram is like that of n-type silicon. At the left side of the junction, it is the energy band diagram of a metal (The Fermi level, E_F , is the energy level when no voltage is applied across the junction.).

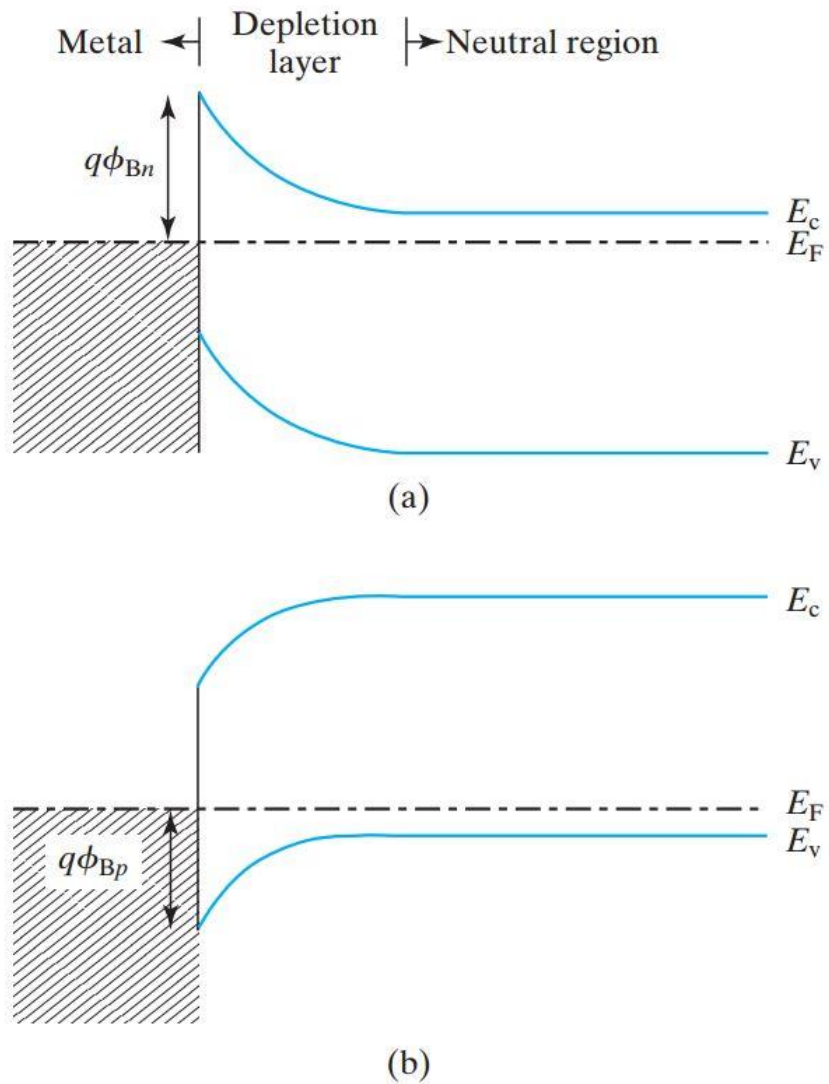


Figure 2.4 Energy band diagram of a M-S contact. The Schottky barrier heights depend on the metal and the semiconductor. (a) band diagram of a metal and an n-type semiconductor; (b) band diagram of a metal and a p-type semiconductor.

According to Schottky and Mott (1938), the barrier height between the metal and n-type semiconductor is given by:

$$q\phi_{Bn} = q(\phi_M - \chi_s) \quad (2.1)$$

where, ϕ_{Bn} is the barrier against electron flow between the metal and n-type semiconductor, ϕ_M is the work function of the metal, χ_s is the electron affinity of the semiconductor. Equation (2.1) shows the Schottky-Mott rule of the M-S contact.

The bandgap energy is given by:

$$q(\phi_{Bn} + \phi_{Bp}) = E_g \quad (2.2)$$

E_g is the bandgap energy in the semiconductor, ϕ_{Bp} is the barrier against hole flow between the metal and p-type semiconductor.

In Tables 2.1 and 2.2, some of the approximate values of ϕ_{Bn} and ϕ_{Bp} are presented. Comparing the barrier heights of each material in the table, and combining with Equation (2.2), the sum of ϕ_{Bn} and ϕ_{Bp} is approximately equal to a fixed value = E_g .

Generally, the Schottky barrier heights are different among different metals and semiconductor materials. In the second and fourth line of Table 2.1, it is clear that the barrier height on n-type silicon, ϕ_{Bn} , increases with the increasing work function ϕ_M .

Table 2.1 Schottky Barrier Heights for Electrons on n-type Silicon (ϕ_{Bn}) and for Holes on p-type Silicon (ϕ_{Bp})

Metal	Mg	Ti	Cr	W	Mo	Pd	Au	Pt
ϕ_{Bn} (V)	0.4	0.5	0.61	0.67	0.68	0.77	0.8	0.9
ϕ_{Bp} (V)		0.61	0.50		0.42		0.3	
Work function ϕ_M (V)	3.7	4.3	4.5	4.6	4.6	5.1	5.1	5.7

Source: Beadle, W.E., J. C. Tsai, and R. D. Plummer, Quick Reference Manual for Silicon Integrated Circuit Technology. 1985: New York: Wiley-Interscience

Table 2.2 Schottky Barrier Heights of Metal Silicide

Silicide	ErSi _{1.7}	HfSi	MoSi ₂	ZrSi ₂	TiSi ₂	CoSi ₂	WSi ₂	NiSi ₂	Pd ₂ Si	PtSi
ϕ_{Bn} (V)	0.28	0.45	0.55	0.55	0.61	0.65	0.67	0.67	0.75	0.87
ϕ_{Bp} (V)			0.55	0.55	0.49	0.45	0.43	0.43	0.35	0.23

Source: Beadle, W.E., J. C. Tsai, and R. D. Plummer, Quick Reference Manual for Silicon Integrated Circuit Technology. 1985: New York: Wiley-Interscience

Research on the influencing factor of barrier heights has been performed over decades. From many experiments and calculations, scientists find that besides the voltage, the temperature can also influence the barrier height [11]. The numerical relationship between the barrier height and the voltage is given by:

$$\frac{d\phi_B}{dT} = \gamma \left[\frac{d\phi_M}{dT} - \frac{d\chi_s}{dT} - \frac{dE_g}{dT} \right] + \frac{dE_g}{dT} \quad (2.3)$$

where, γ is a weighting factor that mainly depends on the condition of the surface [11].

If $\gamma \ll 1$ or $\frac{d(\phi_M - \chi_s)}{dT} \approx \frac{dE_g}{dT}$, Equation (2.3) can reduce to:

$$\frac{d\phi_B}{dT} \approx \frac{dE_g}{dT} \quad (2.4)$$

Equation (2.4) shows that under some exact conditions, the relationship between the temperature T and the barrier height ϕ_B can be approximately described as a linear relationship.

Table 2.3 Relationship between Barrier Heights, Temperature and Voltage

		U(V)									
		0.053		0.100		0.158		0.200		0.263	
T(K)	$\phi_b(T, U)$ cal.(eV)	$\phi_b(T, U)$ com.(eV)									
282	0.7159	0.7156	0.6998	0.6988	0.6892	0.6781	0.6615	0.6630	0.6416	0.6405	
298	0.7459	0.7420	0.7339	0.7252	0.7055	0.7045	0.6878	0.6894	0.6726	0.6669	
316	0.7848	0.7717	0.7724	0.7549	0.7336	0.7342	0.7215	0.7191	0.6932	0.6966	
334	0.8049	0.8014	0.7774	0.7846	0.7623	0.7639	0.7386	0.7488	0.7070	0.7263	
357	0.8402	0.8394	0.8242	0.8225	0.8046	0.8018	0.7708	0.7868	0.7510	0.7643	

Source: Ravindra, N. M., K.S. Kumar, and V. K. Srivastava, Temperature and voltage dependence of the barrier height in SnO₂/Si solar cells. *physica status solidi (a)*, 1982. 70(2): p. 623-630

2.2.2 Thermionic Emission Theory

Thermionic emission means that the flow of charge carriers is induced from the surface. The reason of this phenomenon is that the temperature of the metal provide the energy to the charge carriers [12].

On the basis of the Fermi-Dirac distribution, in the classic image, a free electron gas will escape from the surface of the metal when the energy is over the energy barrier [12].

The quantitative analysis of thermionic emission can be based on the Richardson's law.

The equation is given by:

$$J = A_G T^2 e^{-\frac{W}{kT}} \quad (2.5)$$

where, J is the emission current density, T is the temperature of the metal, W is the work function of the metal, k is the Boltzmann constant, A_G is a parameter that varies among different materials.

$$A_G = \lambda_R A_0 \quad (2.6)$$

$$A_0 = \frac{4\pi m k^2 e}{h^3} \quad (2.7)$$

where, λ_R is a material-specific correction factor that is typically of the order of 0.5, m is the mass of an electron, e is the charge of an electron, h is the Planck's constant [13].

Equation (2.7) shows that the current density increases with increasing temperature.

In order to clarify that the equation of the Richardson's law is an increasing function over $T > 0$, the function graph of $y = x^2 e^{-\frac{1}{x}}$ is given in Figure 2.5 (compared with the Richardson's equation, in this function, all the constants are set as 1 for convenience).

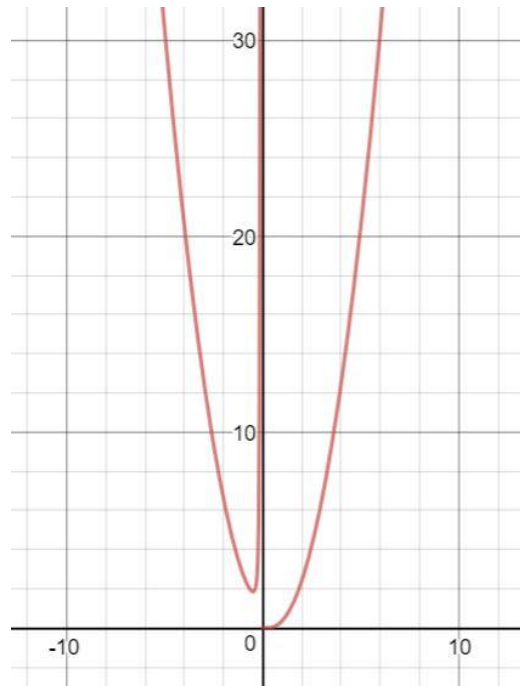


Figure 2.5 Graph of the exponential function $y = x^2 e^{-\frac{1}{x}}$.

CHAPTER 3

ANALYSIS OF THE CURRENT-VOLTAGE AND CAPACITANCE-VOLTAGE MEASUREMENTS

In the past decade, electrical characterization has been investigated and compared for a number of devices [2, 6, 14-17]. This chapter will introduce the measurement of the current-voltage (I-V) and capacitance-voltage (C-V).

3.1 I-V Measurements

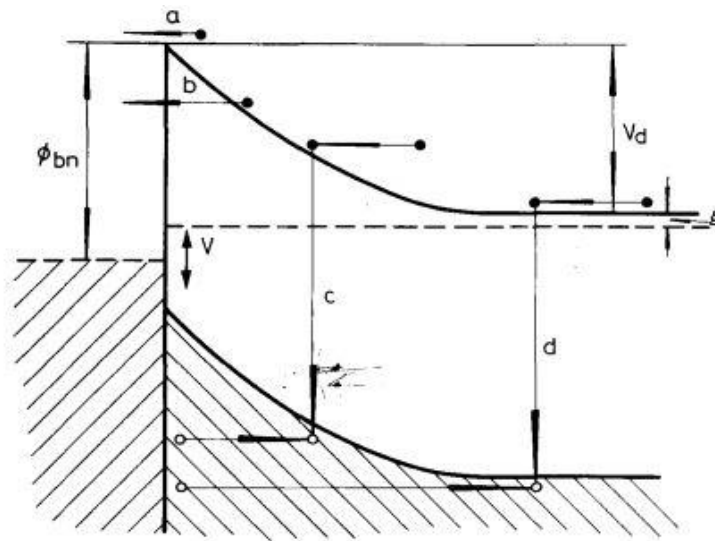


Figure 3.1 Transport processes in forward-biased Schottky barrier on n-type semiconductor.

Source: Rhoderick, E.H., Metal-semiconductor contacts. IEE Proceedings I Solid State and Electron Devices, 1982. 129(1): p. 1.

Figure 3.1 is the schematic of the transport processes under forward-biased voltage.

The schematic includes the following:

- (a) emission of electrons from the semiconductor over the top of the barrier into the metal;
- (b) quantum mechanical tunneling through the barrier;
- (c) recombination in the space-charge region;
- (d) recombination in the neutral region ('hole injection') [18].

Before an electron can be emitted, at first it must be transported through the depletion region of the semiconductor. The emission process is controlled by the number of electrons that impinge on unit area of the metal per second [18].

Using the thermionic-emission theory, it is easy to derive the I-V relationship given by:

$$n = N_c \exp \left\{ -\frac{q(\phi_{Bn} - V)}{kT} \right\} \quad (3.1)$$

where, N_c is the effective density of the states in the conduction band of the semiconductor.

In Chapter 2, a brief introduction to Richardson's law has been given. Utilizing Richardson' law, combining it with the Equation (3.1), the function can be obtained as:

$$I_{semi \rightarrow metal} = A_C K T^2 e^{-\frac{W - qV}{kT}} = I_0 e^{\frac{qV}{kT}} \quad (3.2)$$

$$I = I_{semi \rightarrow metal} + I_{metal \rightarrow semi} = I_0 e^{\frac{qV}{kT}} - I_0 = I_0 (e^{\frac{qV}{kT}} - 1) \quad (3.3)$$

The kinetic theory shows that the flux of the electrons across the interface is $n\bar{v}/4$, where, \bar{v} is the average thermal velocity of the electron in the semiconductor.

Combining Equation (3.1) with Richardson's law, the current density is given by:

$$J = \frac{qN_c\bar{v}}{4} \exp\left(-\frac{q\phi_{Bn}}{kT}\right) \left\{ \exp\left(\frac{qV}{kT}\right) - 1 \right\} \quad (3.4)$$

$$= A^* T^2 \exp\left(-\frac{q\phi_{Bn}}{kT}\right) \left\{ \exp\left(\frac{qV}{kT}\right) - 1 \right\} \quad (3.5)$$

where, $A^* = 4\pi m^* q k^2 / h^3$ is the Richardson constant.

Both functions of the current and the current density shows direct relationship, of not only the voltage applied across the M-S contact, but also the temperature (temperature will influence the magnitude of the current). Furthermore, compared to the voltage, the temperature shows larger influence to the current.

3.2 C-V Measurements

Figure 3.2 gives the schematic of the depletion layer at the Schottky junction. There are two different conditions due to the voltage being applied to the metal or not.

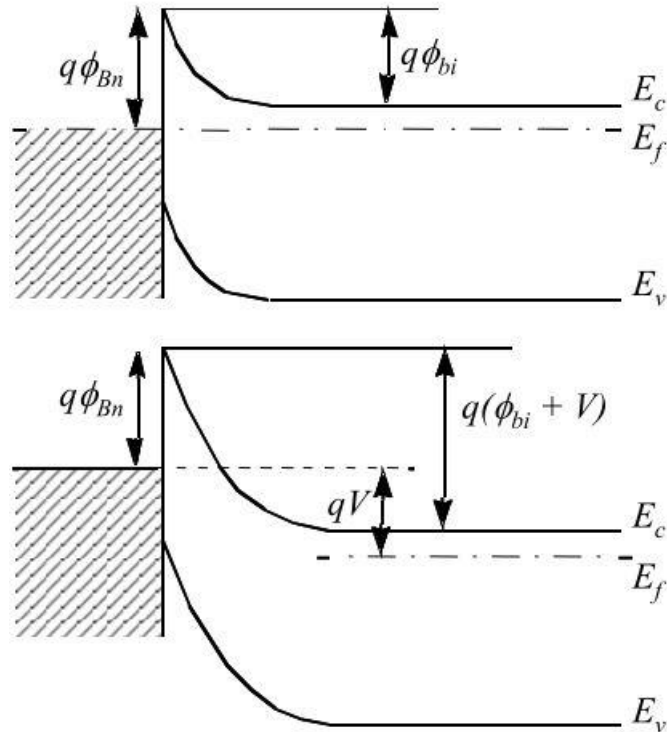


Figure 3.2 Potential across the depletion layer at the Schottky junction. Above: no voltage applied; below: a negative voltage (reverse bias) is applied to the metal.

The depletion-layer thickness is:

$$W_{dep} = \sqrt{\frac{2\epsilon_s(\phi_{bi} + V)}{qN_d}} \quad (3.6)$$

where, ϕ_{bi} is the built-in potential across the depletion layer, ϵ_s is the relative permittivity of the metal, N_d is the donor concentration on the n-side.

For the capacitance, the function for calculation is given by:

$$C = A \frac{\epsilon_s}{W_{dep}} \quad (3.7)$$

where, A is the area of the contact area between metal and semiconductor.

Combining the Equation (3.6) and Equation (3.7), we do some simple calculation.

The relationship between C and V is given by:

$$\frac{1}{C^2} = \frac{2(\phi_{bi} + V)}{qN_d\epsilon_s A^2} \quad (3.8)$$

The plot is shown in Figure 3.3.

It means that if the donor concentration on the n-side, N_d , relative permittivity of the metal, ϵ_s and the contact area A are known, utilizing the C-V plot, we can get the built-in potential ϕ_{bi} .

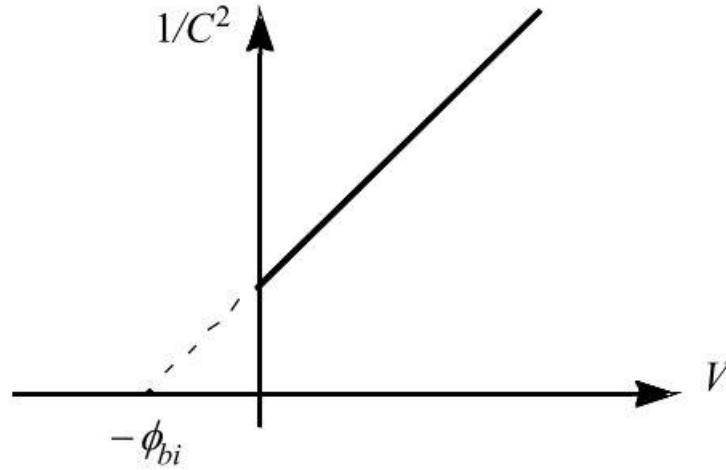


Figure 3.3 The plot of $\frac{1}{C^2}$ versus V on the metal-semiconductor contacts.

Once ϕ_{bi} is known, we can use the relationship between ϕ_{bi} and ϕ_{Bn} :

$$q\phi_{bi} = q\phi_{Bn} - (E_c - E_f) = q\phi_{Bn} - kT \ln \frac{N_c}{N_d} \quad (3.9)$$

where, k is the Boltzmann constant, T is the temperature, N_c is the acceptor concentration on p-side.

Referring to Equation (2.1) in Chapter 2, it is clear that the work function ϕ_M can be calculated. It is given by:

$$\phi_M = \phi_{Bn} + \chi_s \quad (3.10)$$

$$\phi_M = \phi_{bi} + \frac{kT \ln \frac{N_c}{N_d}}{q} + \chi_s \quad (3.11)$$

Equation (3.11) also explains the relationship of temperature to the work function.

As it can be seen, it is a linear relationship.

In 2017, scientists performed small-signal C-V measurements. This results in a modified C-V relationship [in Equation (3.8)]. The plots are shown in Figure 3.4.

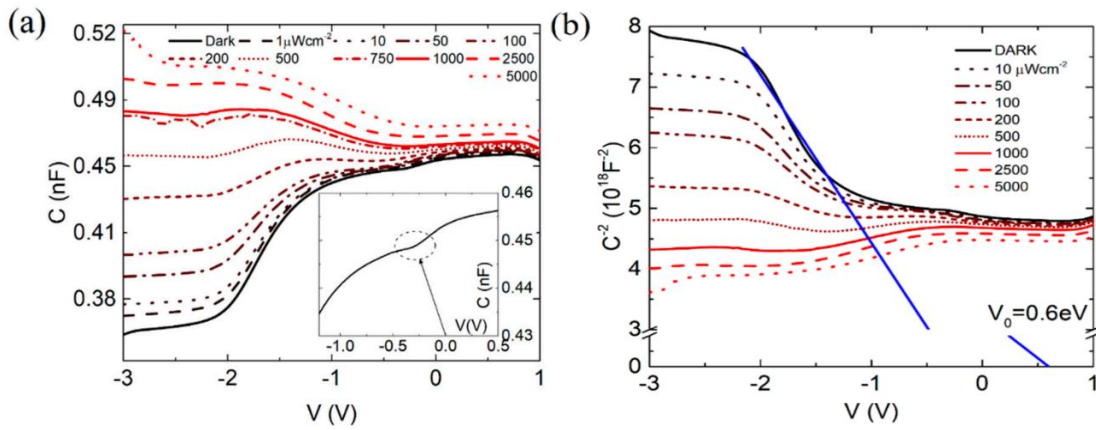


Figure 3.4 (a) Small-signal (100 mV and 10 kHz) C-V plot using Graphene/Si contacts.

(b) the $\frac{1}{C^2}$ -V plot of (a).

Source: Luongo, G., et al., I-V and C-V Characterization of a High-Responsivity Graphene/Silicon Photodiode with Embedded MOS Capacitor. *Nanomaterials* (Basel), 2017. 7(7).

From the plot in Figure 3.4, the barrier height of the material can be calculated.

After the modification, researchers came up with this equation:

$$\frac{1}{C^2} = \frac{2n[n(\phi_{b0} - \phi_{Bn} - kT) - qV]}{qN_d\epsilon_s A^2} \quad (3.12)$$

Under the condition given in the experiment, $\epsilon_s = 11.70\epsilon_0$, $n=3.8$, the calculated value of $\phi_{b0} = 0.47 \text{ eV}$.

CHAPTER 4

PROPERTIES OF MoS₂

Molybdenum disulfide is a compound of molybdenum and sulfur. The chemical formula is MoS₂. MoS₂ is relatively unreactive. Its appearance is like graphite. In daily life, it is often used as a solid lubricant because of its low friction. Bulk MoS₂ is a diamagnetic, indirect bandgap semiconductor; its bandgap is 1.23 eV [19].

4.1 Properties of Bulk MoS₂

4.1.1 Bulk Structure

The bulk structure of MoS₂ is given in Figures 4.1 and 4.2. From Figure 4.2, it can be seen that bulk MoS₂ has a hexagonal structure.

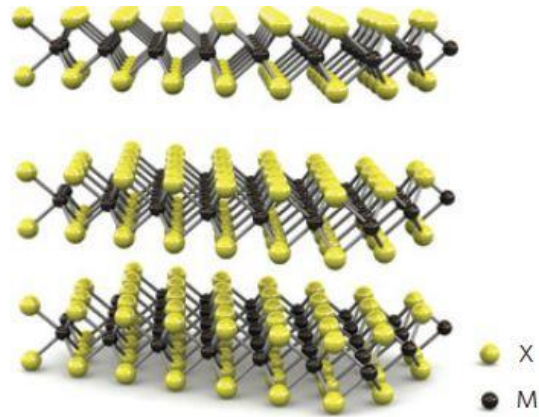


Figure 4.1 Three-dimensional schematic representation of a typical MX_2 structure, with the chalcogen atom (X) in yellow and the metal atom (M) in grey.

Source: Wang, Q.H., et al., Electronics and optoelectronics of two-dimensional transition metal dichalcogenides. *Nat Nanotechnol*, 2012. 7(11): p. 699-712.

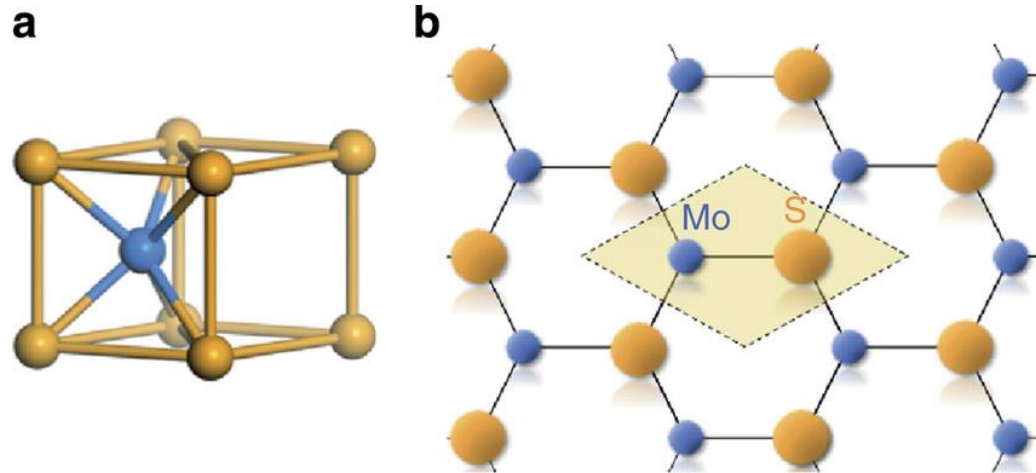


Figure 4.2 (a) Crystal unit cell of MoS₂; (b) top view of the structure of MoS₂

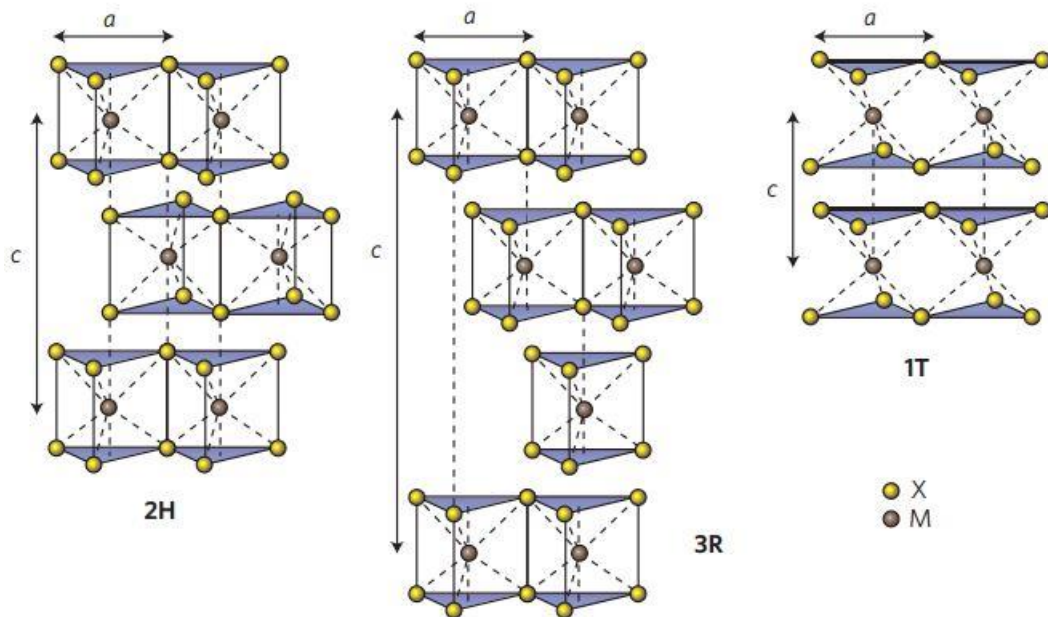


Figure 4.3 Schematics of the structural polytypes: 2H (hexagonal symmetry, two layers per repeat units, trigonal prismatic coordination), 3R (rhombohedral symmetry, three layers per repeat units, trigonal prismatic coordination) and 1T (tetragonal symmetry, one layer per repeat unit, octahedral coordination).

Source: Wang, Q.H., et al., Electronics and optoelectronics of two-dimensional transition metal dichalcogenides. *Nat Nanotechnol*, 2012. 7(11): p. 699-712.

In the schematic of the structure, it shows different combinations of layer structures. These different structures stack in various orders and metal atom coordination. Hexagonal symmetry structure occupies the most part of the structure [20]. In the hexagonal symmetry structure, a chalcogen atom is bounded with three metal atoms. The Van der Waals force between the adjacent layers is weak. This explains why it is often used as a solid lubricant.

Table 4.1 Part of the Physical Properties of Bulk MoS₂

	Molybdenum disulfide
Chemical Formula	MoS ₂
Molar Mass	160.07 g/mole [21]
Density	5.06/cm ³ [21]
Melting Point	1185 °C decomposes
Crystal Structure	hP6, space group P6 3/mmc, No 194(2H) hR9, space group R3m, No 160(3R)
Lattice constant	a=0.3160 nm, c/a=3.89(2H) [22]
Solubility	Insoluble in water [21]

Source: Haynes, W.M., CRC Handbook of Chemistry and Physics. 97th Edition ed. 2016: CRC Press, Wilson, J.A. and A.D. Yoffe, The transition metal dichalcogenides discussion and interpretation of the observed optical, electrical and structural properties. *Advances in Physics*, 1969. 18(73): p. 193-335

4.2 Electronic Properties of Two-Dimensional MoS₂

2D MoS₂ has significantly different properties compared to bulk MoS₂. In this section, we present a detailed comparison. The fabrication of electronic devices for the next generation applications requires conducting and insulating materials, which can achieve higher performance and flexibility [16].

4.2.1 Band Structure

In 2012, Tawinan Cheiwchanchamnangij and Walter R. L. Lambrecht utilized the quasiparticle self-consistent GW method (QS_{GW}) to obtain the band structure of 2D MoS₂ [23-26]. Here G represents the one-electron Green's function and W stands for the screened Coulomb interaction and their product defines the quasiparticle self-energy corrections. They combine this kind of method with the generalized gradient approximation (GGA) to find a transition from an indirect band gap in the bulk and bilayer to a direct band gap in the monolayer MoS₂ [4, 27, 28].

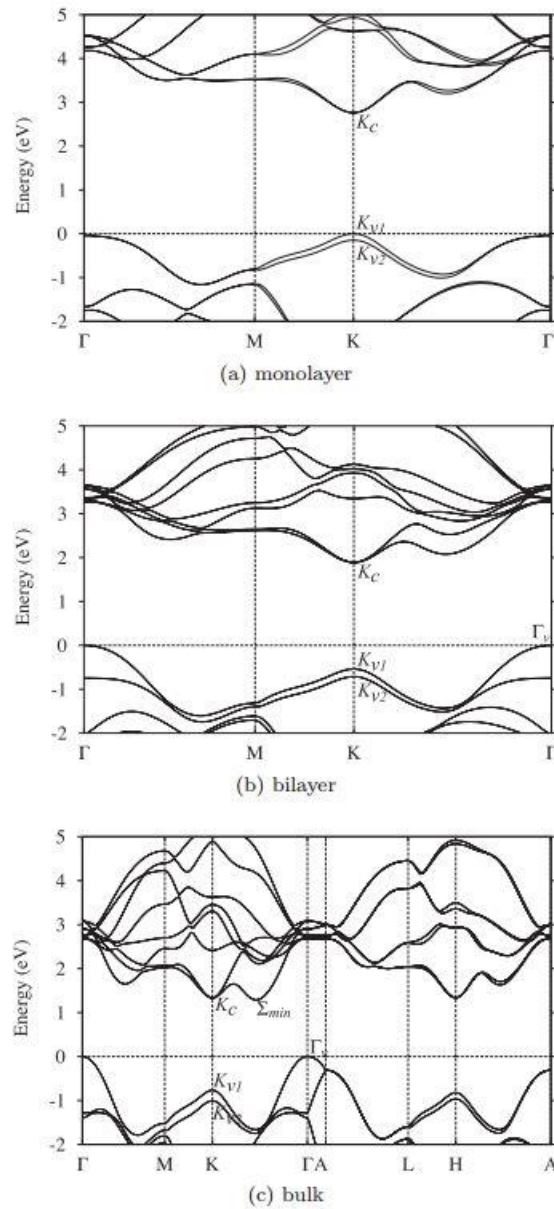


Figure 4.4 Band structure of monolayer (a), bilayer (b), and bulk (c) MoS₂ from QSGW calculations.

Source: Cheiwchanchamnangij, T. and W.R.L. Lambrecht, Quasiparticle band structure calculation of monolayer, bilayer, and bulk MoS₂. *Physical Review B*, 2012. **85**(20).

As shown in Figure 4.4, both bulk and bilayer MoS₂ have indirect band gaps. But the smallest gap of bulk MoS₂ is from Γ to Σ_{min} , where, Σ_{min} is located between K and Γ

points, and the smallest gap of monolayer MoS₂ is at the *K* point. This calculation is in good agreement with experiment results.

The results of calculations, based on QSGW method, is shown in Table 4.2

Table 4.2 Interband Transitions near the Gap in Monolayer, Bilayer and Bulk MoS₂

Structures	Transitions	Transition energy (eV)	
		Calculated	Experiment ^a
Monolayer	K_{v1} to K_c	2.759	1.90
	K_{v2} to K_c	2.905	2.05
Bilayer	Γ_v to K_c	1.888	1.6
	K_{v1} to K_c	2.427	1.88
	K_{v2} to K_c	2.601	2.05
Bulk	Γ_v to Σ_{\min}	1.287	1.29
	K_{v1} to K_c	2.099	1.88
	K_{v2} to K_c	2.337	2.06

Source: Cheiwchanchamnangij, T. and W.R.L. Lambrecht, Quasiparticle band structure calculation of monolayer, bilayer, and bulk MoS₂. Physical Review B, 2012. **85**(20).

The calculations overestimate the direct gap at *K* point by 0.2-0.3 eV in bulk MoS₂, and in the monolayer and bilayer, the value is more than 0.5 eV. The reason for this overestimation is the large excitonic effect in 2D system [23].

Besides these results, another group of scientists have performed research on the band structure of MoS₂ using a different method. In 2013, Wencan Jin, Po-Chun Yeh et al. studied the band gap structure using Angle-Resolved Photoemission Spectroscopy.

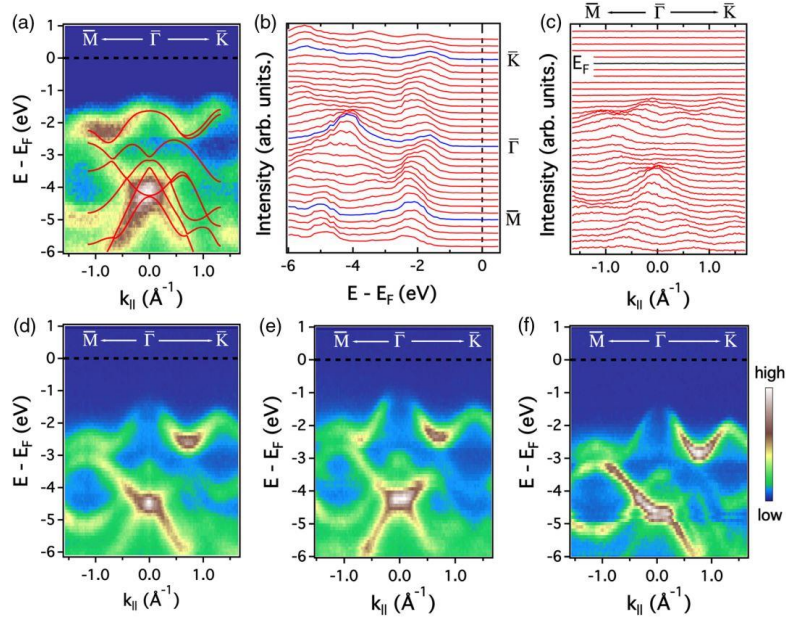


Figure 4.5 (a) Band map of exfoliated monolayer MoS₂ along the high symmetry line. (b)-(c) Corresponding EDCs (energy distribution curves) and MDCs (momentum distribution curves). (d)-(f) band map of exfoliated bilayer, trilayer, and bulk MoS₂, respectively.

Source: Jin, W., et al., Direct measurement of the thickness-dependent electronic band structure of MoS₂ using angle-resolved photoemission spectroscopy. Phys Rev Lett, 2013. **111**(10): p. 106801.

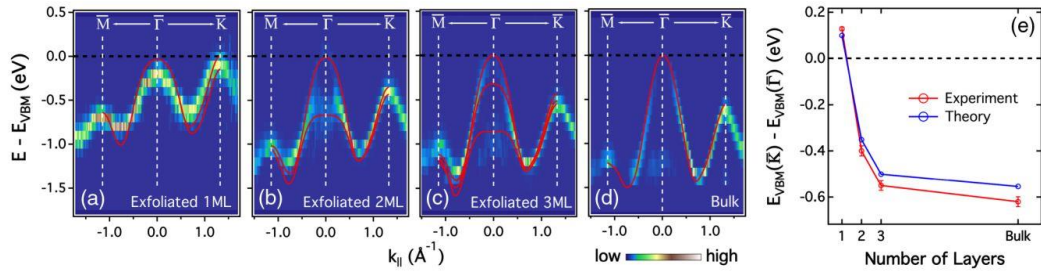


Figure 4.6 (a)–(d) 2D curvature intensity plots of the low energy valence band of exfoliated monolayer, bilayer, trilayer, and bulk MoS₂, respectively. Red curves are the corresponding DFT (density function theory) calculated bands. (e) Thickness dependence of the energy difference between VBM (valence band maximum). The theoretical and experimental results are plotted together for comparison.

Source: Jin, W., et al., Direct measurement of the thickness-dependent electronic band structure of MoS₂ using angle-resolved photoemission spectroscopy. Phys Rev Lett, 2013. **111**(10): p. 106801.

In this study, the Figures 4.5 and 4.6 show the band structure between the different layer size of MoS₂. From Figure 4.6 e, it can be seen that, with increasing number of layers, the energy difference between VBM of \bar{K} and $\bar{\Gamma}$ decreases. This phenomenon is due to the quantum confinement as the number of layers changes. The VBM at \bar{K} (derived from the localized in-plane Mo $d_{x^2-y^2}/d_{xy}$ orbitals) is not likely to be affected by quantum confinements. But the VBM at $\bar{\Gamma}$ (derived from the rather delocalized out-of-plane Mo d_{z^2} orbitals and S_{p_z} orbitals) is lowered in energy when the interlayer interactions increase with increasing number of layers [29].

4.2.2 Influence of Temperature on the Electronic Properties of MoS₂

In the previous section, the structure of MoS₂ was introduced; in order to utilize MoS₂ in devices, circuits and systems, it is critical to understand its electronic properties.

In this section, we will discuss the influence of temperature on the electronic properties of MoS₂.

The electronic properties of MoS₂ are sensitive to temperature. In general, when the temperature increases, its energy gap decreases[30]. The reason for this behavior is that, with increasing energy, the amplitude of vibration (between the atoms) increases. This results in increase in atomic spacing; it decreases the potential energy in the MoS₂ material, resulting in reduced energy gap.

The quantitative analysis of the temperature dependence of the energy gap in MoS₂ is given by the function of a replacement of Varshni's equation[31]:

$$E_g(T) = E_0 - \frac{\alpha T^2}{T + \beta} \quad (4.1)$$

This is the original Varshni relation, where, α and β are fitting parameters, characteristic of a given material, and E_0 is the energy gap at 0 K.

In this study, the researchers, K. P. O'Donnell and X. Chen, proposed a replacement of Varshni's equation.

$$E_g(T) = E_g(0) - S\langle\hbar\omega\rangle \left[\coth\left(\frac{\langle\hbar\omega\rangle}{2kT}\right) - 1 \right] \quad (4.2)$$

where, $E_g(0)$ is the band gap at 0 K. S is a dimensionless constant, $\langle\hbar\omega\rangle$ is the average phonon energy.

In the literature, researchers have performed experiments on various semiconductors including gallium arsenide (GaAs), gallium phosphide (GaP), silicon (Si) and diamond. Figure 4.7 shows the variation of band gap with temperature for four different semiconductors [32].

The parameters of the temperature dependence of the energy gap of 2D MoS₂ are presented in Table 4.3.

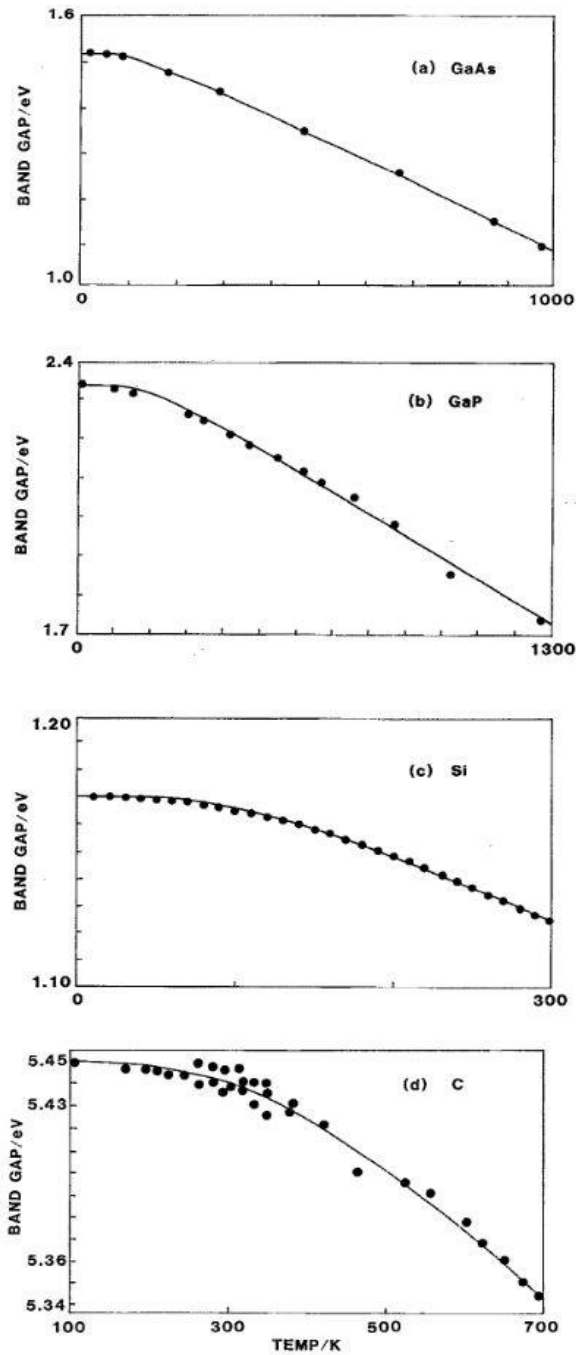


Figure 4.7 Energy band gaps as a function of temperature of (a) GaAs, (b) GaP, (c) Si and (d) diamond.

Source: O'Donnell, K.P. and X. Chen, Temperature dependence of semiconductor band gaps. Applied Physics Letters, 1991. **58**(25): p. 2924-2926

Table 4.3 Parameters for temperature dependence of energy gap of 2D MoS₂

Material	MoS ₂
$E_g(0)$ (eV)	1.86
S	1.82
$\langle \hbar\omega \rangle$ (10^{-3} eV)	2.25

Source: Tongay, S., et al., Thermally driven crossover from indirect toward direct bandgap in 2D semiconductors: MoSe₂ versus MoS₂. Nano Lett, 2012. **12**(11): p. 5576-80.

By analyzing Equation (4.2), and replacing the parameters with the data in Table 4.3, it is observed that the relationship between the temperature and the energy band gap is almost linear.

4.3 Optical Properties of Two-Dimensional MoS₂

2D structure of MoS₂ has different optical properties compared to other 2D semiconductors due to the weakly bonded atoms by Van der Waals force [33, 34]. In the experiments, scientists utilized Raman spectroscopy to study the optical properties of layered transition metal dichalcogenides (LMDCs), such as MoS₂, MoSe₂, WSe₂ etc.

4.3.1 Raman Spectroscopy

Raman spectroscopy is a technique that is utilized to observe the vibrational, rotational and other low-frequency modes in the system [35-37]. It relies on the Raman effect also known

as Raman scattering; it is the inelastic scattering of photons that are excited to higher vibrational or rotational energy levels. The scattering is usually caused by the interaction of photons, from a laser in the range from near infrared to near ultraviolet, with materials [35, 36].

The photons from the laser interact with molecular vibrations, i.e., phonons, and cause the energy of the laser photons to be shifted up or down. From the energy changes, scientists can get information on the vibrational modes in the system [35, 36].

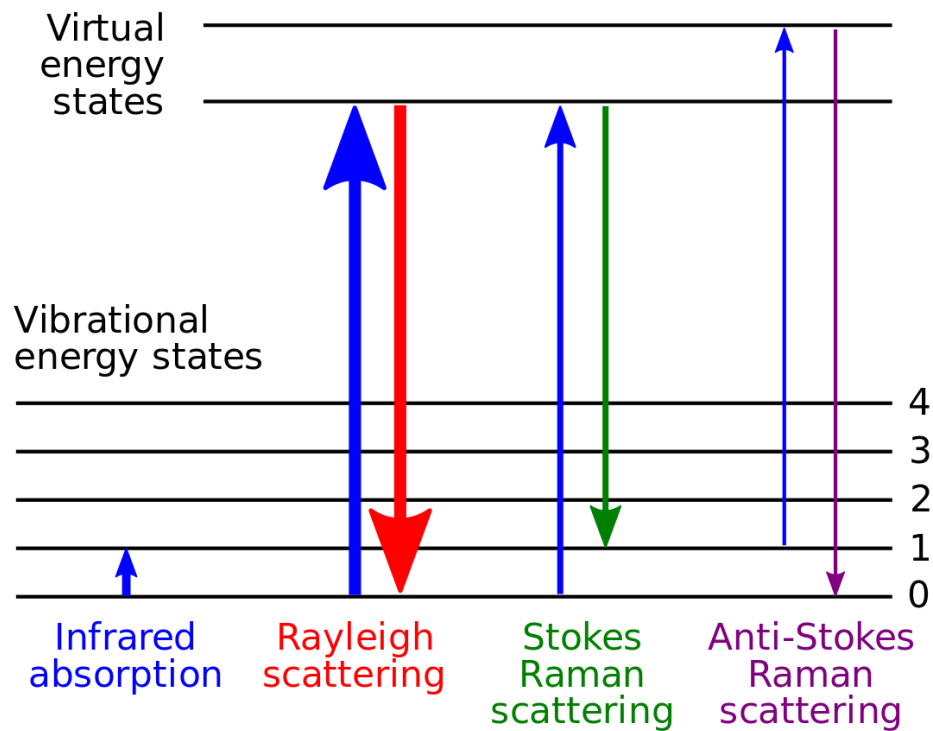


Figure 4.8 Energy level diagram showing the states involved in Raman spectra.

Source: Moxfyre, Molecular energy levels and Raman effect, R.e. levels.jpg, Editor. 2009.

The Raman effect is based on the interaction of the electron cloud and the external electromagnetic radiation due to the field of light. The light can induce dipole moment based on polarizability.

If the final state has higher energy than the initial state, the scattered photons will have a lower frequency (lower energy) to remain at the same energy. It is called the Stokes shift. In contrast, if the final state has lower energy, the frequency will increase. It is known as the anti-Stokes shift.

4.3.2 Experiment

In 2013, K. Gołasa, M. Grzeszczyk et al., performed experiments using Raman Spectroscopy to observe the monolayer MoS₂. In Figures 4.9 - Figure 4.12, the Raman spectra of monolayer MoS₂ are presented.

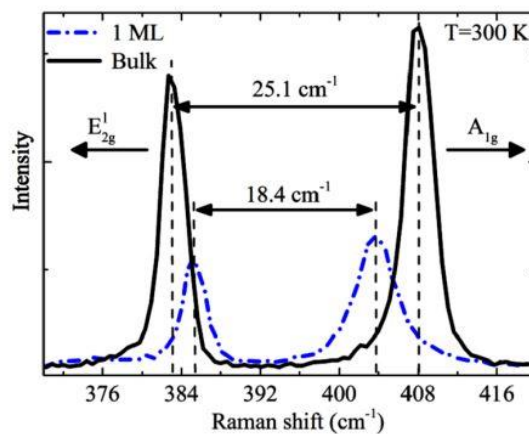


Figure 4.9 Raman active modes in the bulk material and monolayer MoS₂.

Source: Gołasa, K., et al., Optical Properties of Molybdenum Disulfide (MoS₂). Acta Physica Polonica A, 2013. 124(5): p. 849-851.

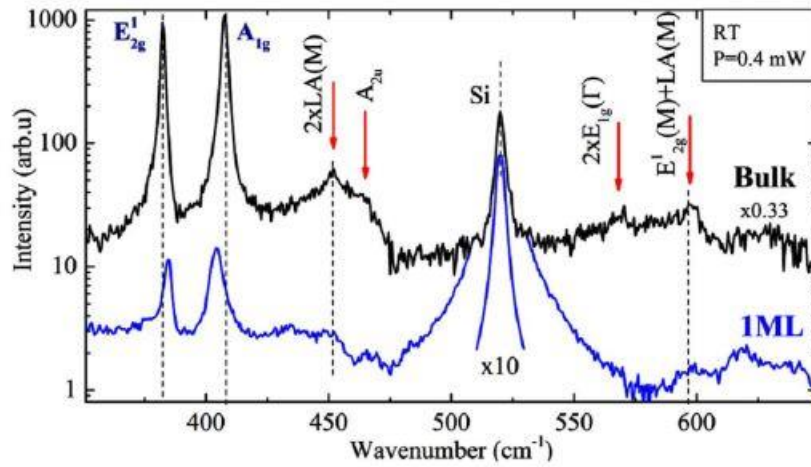


Figure 4.10 Non-resonance room-temperature Raman scattering spectra from the bulk and monolayer MoS₂.

Source: Gołasa, K., et al., Optical Properties of Molybdenum Disulfide (MoS₂). Acta Physica Polonica A, 2013. 124(5): p. 849-851.

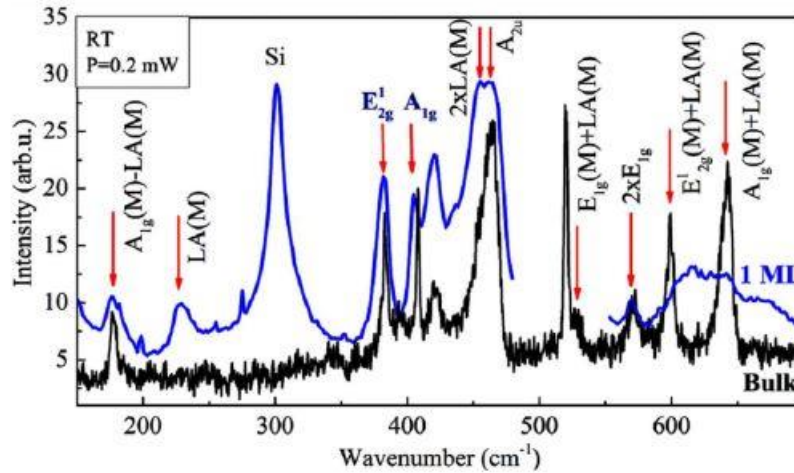


Figure 4.11 Room-temperature Raman scattering spectra from the bulk and monolayer MoS₂ with the resonant (632.8 nm) excitation.

Source: Gołasa, K., et al., Optical Properties of Molybdenum Disulfide (MoS₂). Acta Physica Polonica A, 2013. 124(5): p. 849-851.

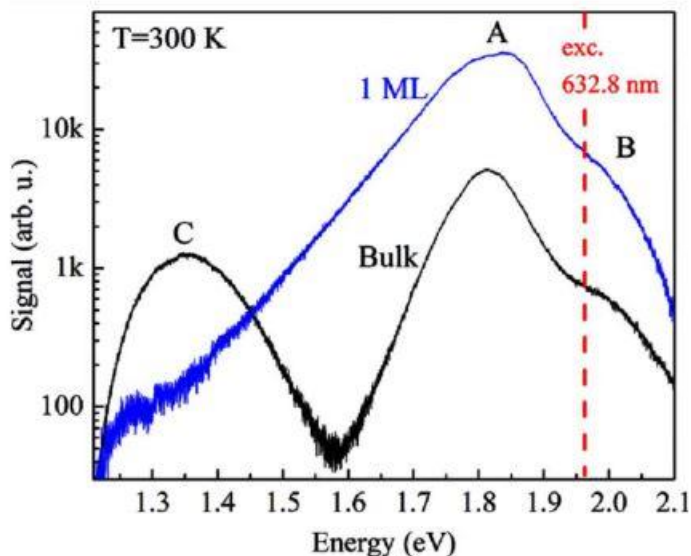


Figure 4.12 Room-temperature photoluminescence spectra in the bulk material and monolayer MoS₂. Measurements were performed with a non-resonant excitation ($\lambda = 532$ nm).

Source: Gołasa, K., et al., Optical Properties of Molybdenum Disulfide (MoS₂). *Acta Physica Polonica A*, 2013. 124(5): p. 849-851.

The figures, 4.9-4.12 present the significant difference between the Raman spectrum properties of the bulk and monolayer MoS₂. It means that the rotation and vibration modes of these two kinds of materials are very different. It can be explained by the disorder in the monolayer MoS₂.

4.4 Preparation of Two-Dimensional MoS₂

Preparation of monolayer MoS₂ can be accomplished using “Scotch tape method” [9].

However, in this method, it is hard to control the size of the sheet and layer number [34].

In 2012, Karim Gacem and other scientists found a new technique to do it [38].

They used the anodic bonding technique that is based on an apparatus shown in Figure 4.13. This work has helped researchers to obtain several-layered materials.

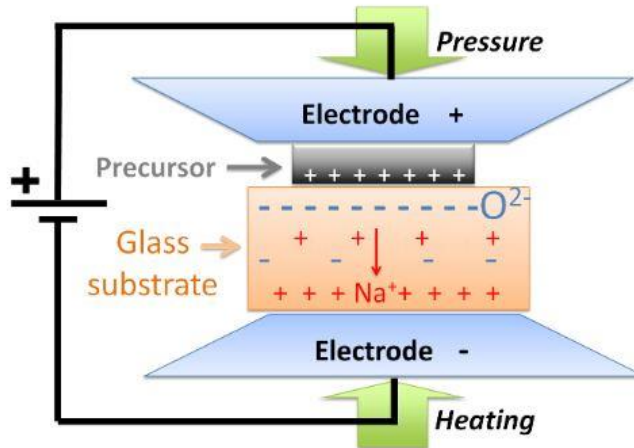


Figure 4.13 Schematic of the Anodic Bonding principle.

Source: Gacem, K., et al., High quality 2D crystals made by anodic bonding: a general technique for layered materials. *Nanotechnology*, 2012. **23**(50): p. 505709.

An example of the anodic bonding technique is described here. At high temperature (~ 473 K), Na_2O decomposes into O^{2-} and Na^+ . Na^+ ions migrate to the cathode at its back. The negative space charge accumulates on the surface. The electric field created due to the positive and negative charges will lead to a strong electrostatic bonding between the two materials and Si-O-Si will form [38].

This technique can be adapted to obtain monolayers. At appropriate temperatures, graphene layers can be obtained after the graphite precursor has been peeled off mechanically.

Under the observation by atomic force microscopy (AFM), measurements of carrier

mobility and quantum Hall effect, the researchers believe that this technique can lead to monolayer structures with characteristics similar to the structure obtained by scotch tape graphene [38].

CHAPTER 5

METAL-MoS₂ CONTACTS

In this chapter, we will introduce various metal-semiconductor contacts on MoS₂. Metal-MoS₂ contacts are widely used in the semiconductor industry. These devices have unique properties compared to other metal-semiconductor contacts in electronic, thermal and optoelectronic applications.

5.1 Properties

In Figure 5.1, the graph shows the band structure of MoS₂ and metals such as Cu, Ag, Au, Pt. In addition, it also gives the band structure of their corresponding metal-MoS₂ contacts.

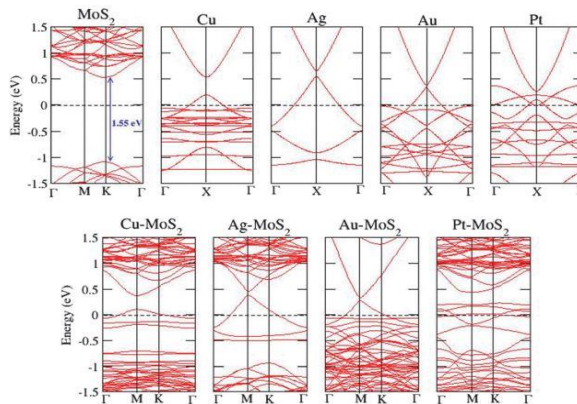


Figure 5.1 Electronic band structure of (top panel) the pristine monolayer, wires and (down panel) the assembly.

Source: Kumar, A., et al., Electronic stability and electron transport properties of atomic wires anchored on the MoS₂ monolayer. *Phys Chem Chem Phys*, 2014. **16**(37): p. 20157-63.

In Figure 5.1, it shows that the MoS₂ monolayer has a band gap of 1.55eV at *K* point. For the metal/MoS₂ monolayer, the valence band is associated with the Mo-d and S-p state. The metals retain their bands in the monolayer. The reduction in the energy difference by 0.5 eV is due to the partially occupied bands in the metal atom.

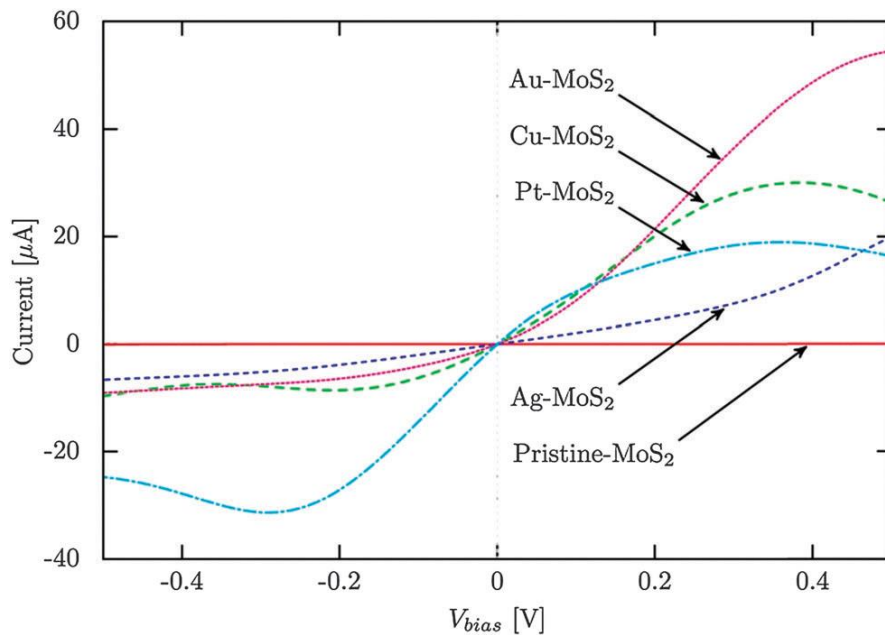


Figure 5.2 The current–voltage (I–V) characteristics of pristine and assembled monolayers.

Source: Kumar, A., et al., Electronic stability and electron transport properties of atomic wires anchored on the MoS₂ monolayer. *Phys Chem Chem Phys*, 2014. **16**(37): p. 20157-63.

Scientists have performed the analysis of current-voltage characteristics of several metal-MoS₂ contacts under bias voltage (from -0.5 V to 0.5 V). As can be seen in Figure 5.2, the currents are not increasing function of bias voltage. Under reverse bias, except Pt-MoS₂, other metal-MoS₂ devices exhibit nearly constant current. In forward bias, the

current in Au-MoS₂ increases rapidly, the current is likely a linear function of the bias voltage. The currents in Cu-MoS₂ and Pt-MoS₂ increase slower than in Au-MoS₂. The current in Ag-MoS₂ increases faster when the bias voltage is higher than 0.3 V. The current in pristine-MoS₂, with no metal, shows no change in current under varying voltage.

These variations in the current-voltage characteristics of metal-MoS₂ contacts have been attributed to their band structure. Considering Pt-MoS₂, the appearance of unoccupied states contributes to the large tunneling current under reverse bias. The larger occupied states between 0 to -0.5 V causes larger current in Au-MoS₂ than in Ag-MoS₂ [16].

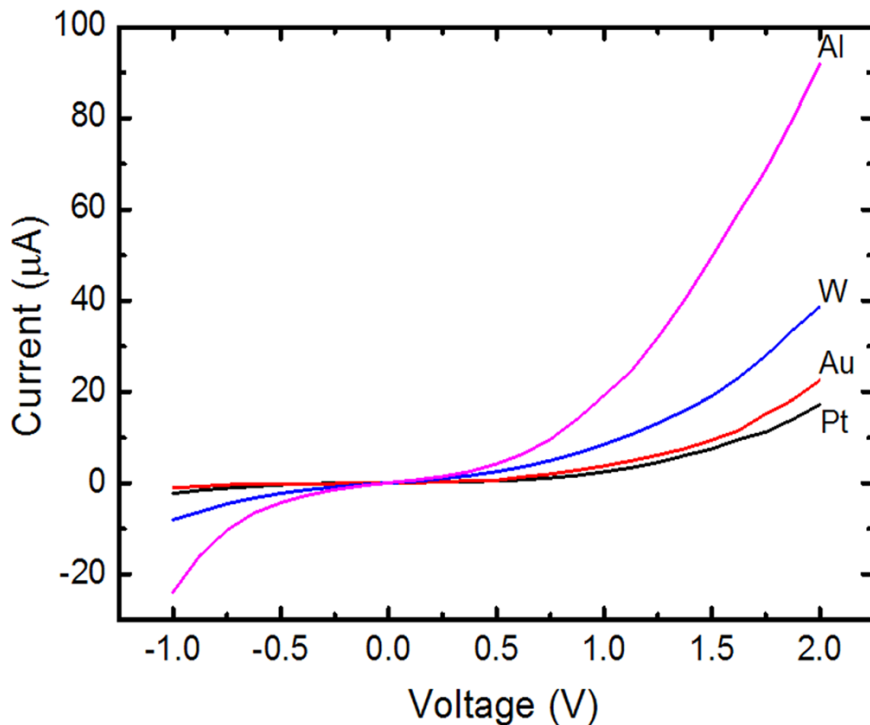


Figure 5.3 I-V characteristics for different metal-MoS₂ contacts.

Source: Walia, S., et al., Characterization of metal contacts for two-dimensional MoS₂ nanoflakes. Applied Physics Letters, 2013. **103**(23): p. 232105.

A different group of scientists [41] has also performed I-V measurements; this group used the liquid exfoliation method [39-41]. Comparing the two results, in Figures 5.2 and 5.3, we notice significant differences between them.

In both the groups, scientists studied Au-MoS₂ and Pt-MoS₂; here, we will compare these two groups of metal-MoS₂ contacts.

Table 5.1 Comparison of Two Different I-V Characteristics of Au-MoS₂ Contact (I₁: the current data from Figure 5.2, I₂: the current data from Figure 5.3)

Bias Voltage (V)	-0.50	-0.40	-0.27	0.11	0.2	0.5
I₁ (μA)	-9.10	-8.44	-7.44	8.47	10.44	12.35
I₂ (μA)	-0.21	-0.22	-0.14	0.01	0.45	0.56

Table 5.2 Comparison of Two Different I-V Characteristics of Pt-MoS₂ Contact (I₁: the current data from Figure 5.2, I₂: the current data from Figure 5.3)

Bias Voltage (V)	-0.50	-0.40	-0.27	0.11	0.2	0.5
I₁ (μA)	-25.10	-28.15	-31.46	10.30	14.86	16.33
I₂ (μA)	-0.69	-0.40	-0.23	0.0003	0.0012	0.21

We chose several points from each graph; the corresponding points are for the same bias voltage.

In Tables 5.1 and 5.2, above, we can clearly see the differences in the data obtained

by the two different experiments. For the same bias voltage, the current magnitudes of I_1 are much larger than the current magnitudes of I_2 . The curves in Figure 5.3 can be described by hyperbolic cosine function. However, the curves in Figure 5.2 show that they are not a strict increasing function; this is an interesting phenomenon for researchers to study.

The reasons for this obvious difference in the current-voltage characteristics maybe the method of comparison of two-dimensional materials or different metals on the substrates. The exact reason needs to be clarified in future research.

For metal-semiconductor contacts, the work function is a very important characteristic. It is the minimum energy required to move an electron in a solid to the vacuum level.

In the band structure, the metal does not have a band gap, and the semiconductor has the band gap lower than 3 eV in general. The bulk MoS_2 has an indirect band gap.

From the schematic in Figure 5.4, it is clear that, after establishing the contact, the electrons near the contact point gradually diffuse from the original higher energy state to the lower state. The total energy state of the semiconductor (MoS_2) decreases. After establishing the contact, a barrier, known as the Schottky Barrier, is formed against the migration of the electrons. Due to the Schottky-Mott rule, described in Chapter 2, it can be understood that a higher metal work function will cause a higher Schottky barrier height.

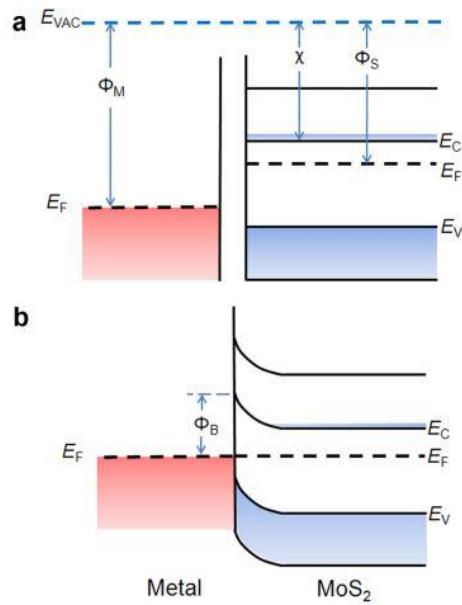


Figure 5.4 Band structure of metal and MoS₂ for work function (ϕ_M) > electric affinity (χ) (a) before establishing a contact and (b) after establishing the contact. E_F is the Fermi level of MoS₂, E_C is the conduction band level.

Source: Walia, S., et al., Characterization of metal contacts for two-dimensional MoS₂ nanoflakes, Applied Physics Letters, 2013. **103**(23): p. 232105.

5.2 Applications

Metal-2D MoS₂ contacts can make it possible to design ultra-thin FET, MOS and TMDC.

In the previous chapters, we introduced the electronic and optical properties of MoS₂. Utilizing these significant properties, scientists and engineers have designed a significant number of devices.

Sumeet Walia and collaborators have calculated the work function of several metal-MoS₂ contacts. They chose the 2D structure of MoS₂; this data is summarized in Table 5.3.

Table 5.3 Performance of Different Metal/2D MoS₂ Contacts

Metal	Work function(eV)	Schottky barrier height $\phi_{Bn} = \phi_M - \chi_s$ (eV)	Current at +2 V bias (μ A)
Al	4.5	0.5	91.9
W	5.1	1.1	38.7
Au	5.4	1.4	22.5
Pt	5.7	1.7	17.3

Source: Walia, S., et al., Characterization of metal contacts for two-dimensional MoS₂ nanoflakes. Applied Physics Letters, 2013. 103(23): p. 232105.

In Table 5.3, it is shown that as one of the candidates, Al-MoS₂ contact has the much larger current under the same bias voltage. It is related to the lower Schottky barrier height. Al-MoS₂ has the lower work function; it results in Al-MoS₂ having a lower barrier height so that a lower forward bias is required to overcome the Schottky barrier height. This leads to the consequence that the Al-MoS₂ device can switch faster than other metal-semiconductor contacts; scientists and engineers can utilize such materials to improve the performance and response speed of the system.

The mobility of the metal-MoS₂ contact is much larger compared to the other metal-semiconductor contacts used in the semiconductor industry. At room temperature, the carrier density is about $10^{13}/\text{cm}^2$ [42]. Compared to other candidates, it is at least 5 times greater.

The contact resistance varies with different substrates and temperature. Due to such characteristics, it can be used in the temperature-controlled devices.

The metal-semiconductor device is very thin compared with other devices; therefore, scientists have been able to develop thin-film-transistor liquid-crystal displays (TFT LCDs).

CHAPTER 6

FUNCTIONAL FORM OF CURRENT-VOLTAGE CHARACTERISTICS

In this Chapter, we introduce the functional form of current-voltage characteristics of metal-semiconductor contacts.

In this research, WebPlotDigitizer is used as a tool to obtain the data points from the figures in the literature. COMSOL is utilized as a simulation tool to simulate the electronic properties of metal-semiconductor contacts.

The data from Figures 5.2 and 5.3 is digitized. The fitting results are summarized in the Appendix.

From the several groups of I-V curves, we have attempted to verify the functional relationship between current and bias voltage applied across the metal-MoS₂ contacts. Here, we perform linear, quadratic and cubic fitting method on the graphs.

The quadratic fitting and cubic fitting are better than the linear fitting in both the simulations. The graph shows that the current is increasing with increasing voltage. For different metal-semiconductor contacts, the fitting functions are different; this is due to the properties of the metal.

CHAPTER 7

CONCLUSIONS

2D materials and metal-semiconductor contacts are widely utilized in the industry in the form of devices, circuits and systems. In this research, we mainly focus on MoS₂ and its metal-semiconductor contacts and their properties, such as the barrier height, the Raman spectra, the I-V and C-V characteristics.

MoS₂ is a semiconductor that has an indirect band gap. From this research, the results indicate that MoS₂ and its metal-semiconductor contacts are very sensitive to voltage and temperature. The I-V characteristics and C-V characteristics indicate that both the relationships are nonlinear; this is different from the Ohmic contact. This characteristic makes it possible to use metal-semiconductor contacts in temperature-controlled area and circuits and systems that are needed to control the voltage in a small range. Comparing the different metal-MoS₂ contacts, it can be determined that the work function and barrier heights vary among the contacts.

The metal-MoS₂ contacts are studied. The I-V relationships from two research groups show different results. The exact reasons need to be verified in future research.

In research, the method of preparation is also important. The Scotch tape method is briefly mentioned. This method is simple, but under some other condition, it is not easy to achieve exfoliating of MoS₂. In this research, we mainly discuss Karim Gacem's method,

which is called anodic bonding. Compared to the Scotch tape method, it can prepare controllable and large size of few-layer MoS₂, and the size can range from 10 μm to several hundred microns. There are also many other methods, such as CVD (Chemical Vapor Deposition) synthesis, Sulfurization of Mo and Mo based oxides, vapor-solid growth from MoS₂ powder etc. [34].

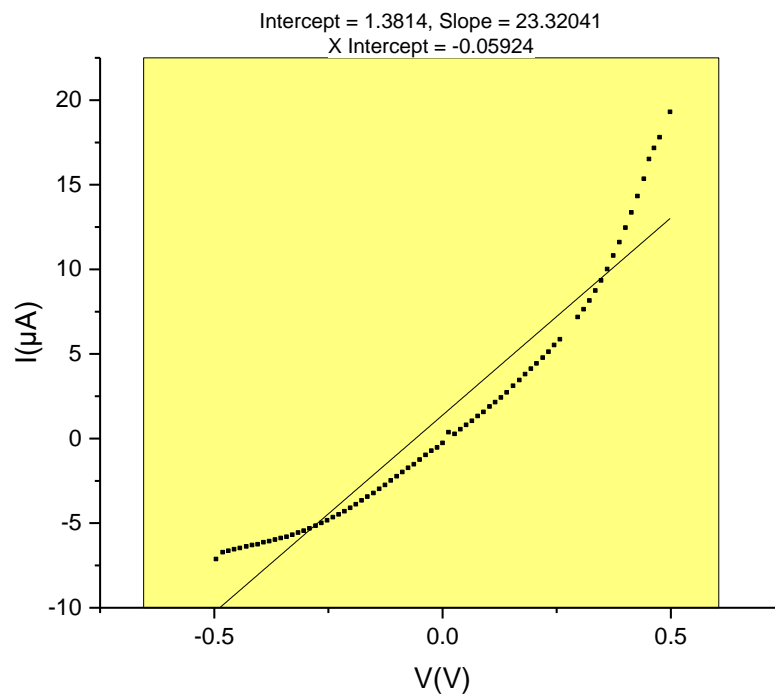
MoS₂ can operate at fast switching speeds due to the lower forward voltage; it makes it possible to use them in the FET (field-effect transistor) and TMDCs (Transition metal dichalcogenides).

In conclusion, MoS₂ material, especially its 2D structure has many significant properties compared to other materials. Related research is very popular in materials science.

APPENDIX

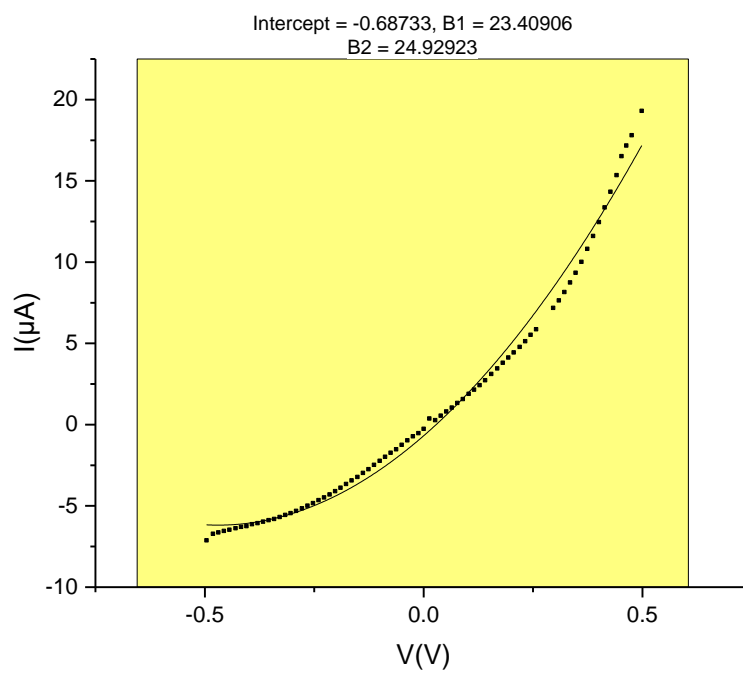
In this section, we will summarize the results of several fitting methods that have been performed to fit the curves in Figures 5.2 and 5.3. We have attempted to describe the functions in polynomial function form.

Figures A.1 to A.4 are the fitting results obtained from Figure 5.2.

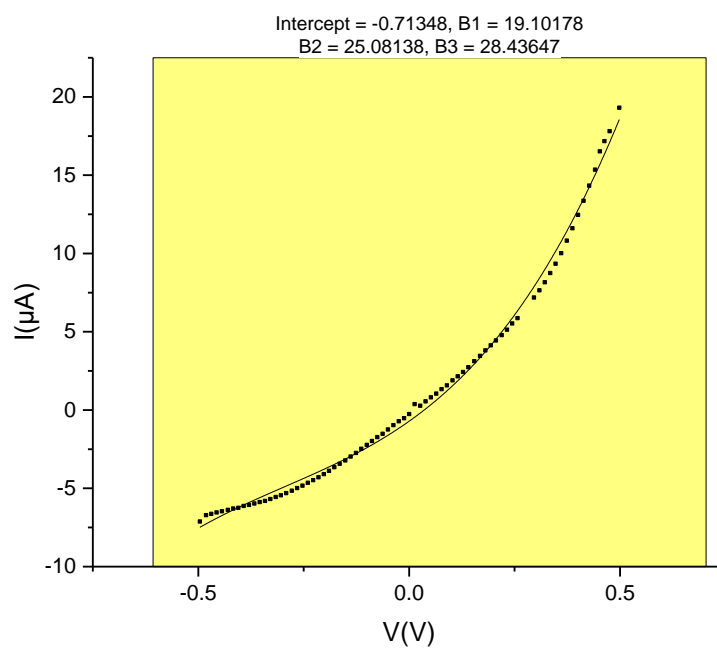


(a)

Figure A.1 Ag-MoS₂ current-voltage characteristic curves (a) linear fitting; (b) quadratic fitting; (c) cubic fitting (Continued).

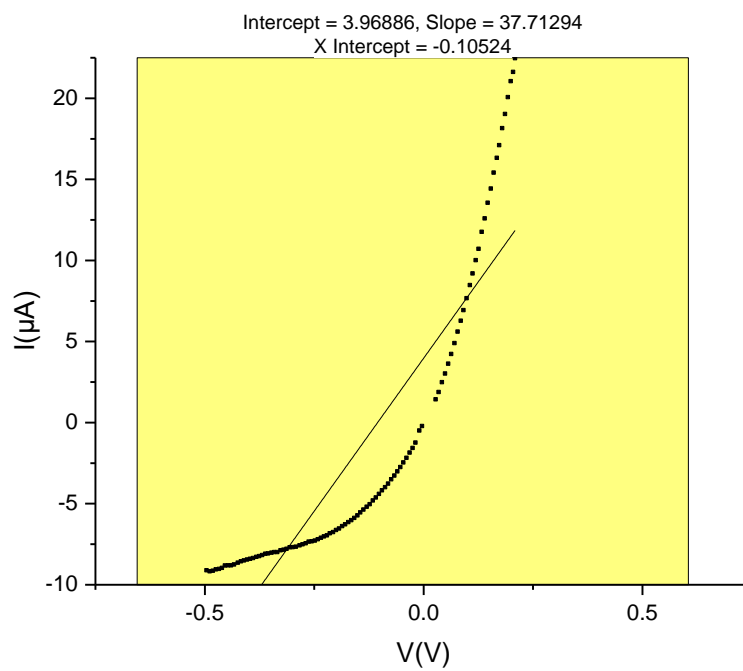


(b)

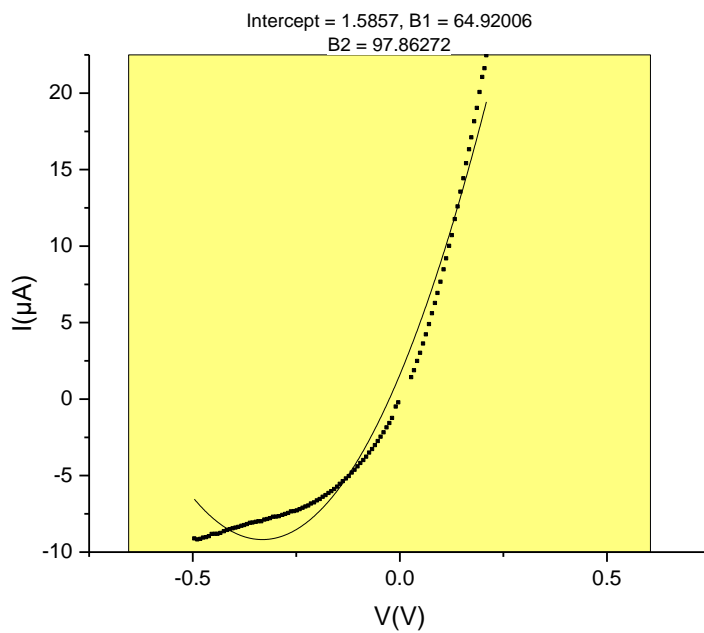


(c)

Figure A.1 (Continued) Ag-MoS₂ current-voltage characteristic curves (a) linear fitting; (b) quadratic fitting; (c) cubic fitting.

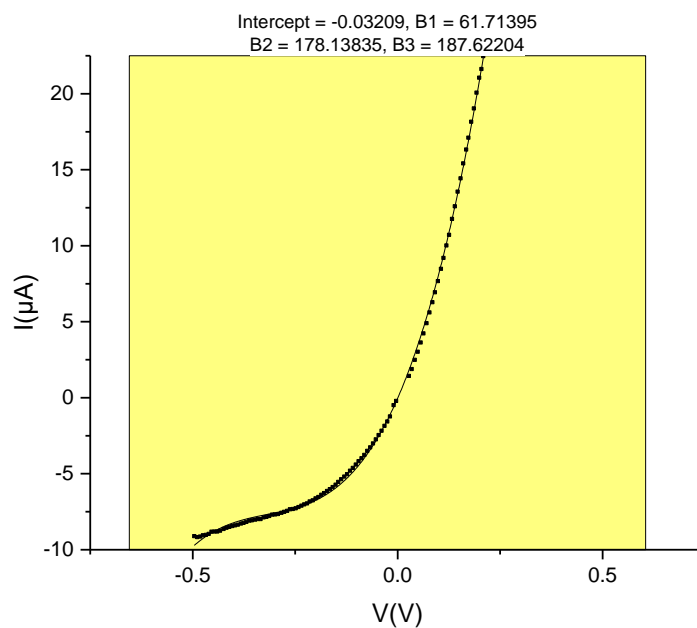


(a)



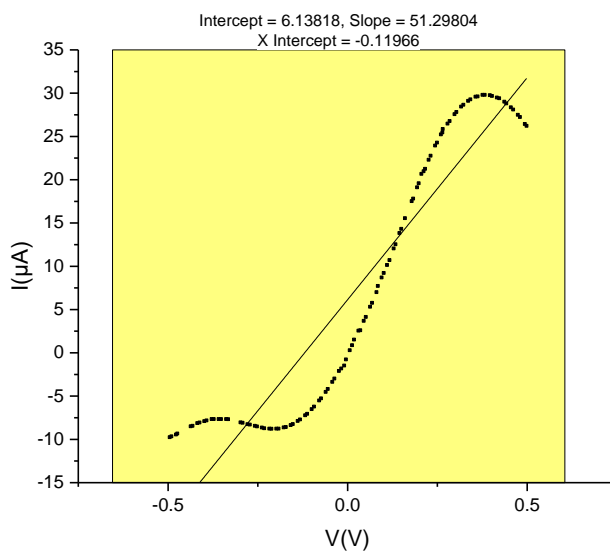
(b)

Figure A.2 Au-MoS₂ current-voltage characteristic curves (a) linear fitting; (b) quadratic fitting; (c) cubic fitting (Continued).



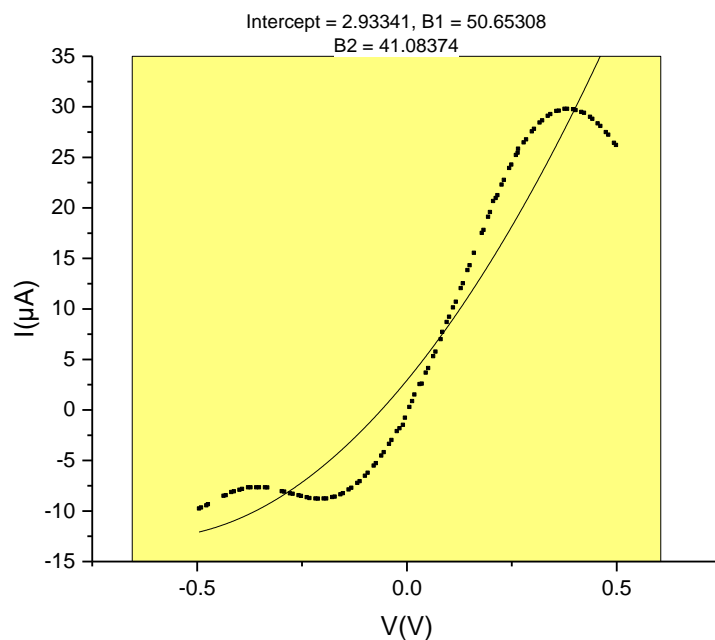
(c)

Figure A.2 (Continued) Au-MoS₂ current-voltage characteristic curves (a) linear fitting; (b) quadratic fitting; (c) cubic fitting.

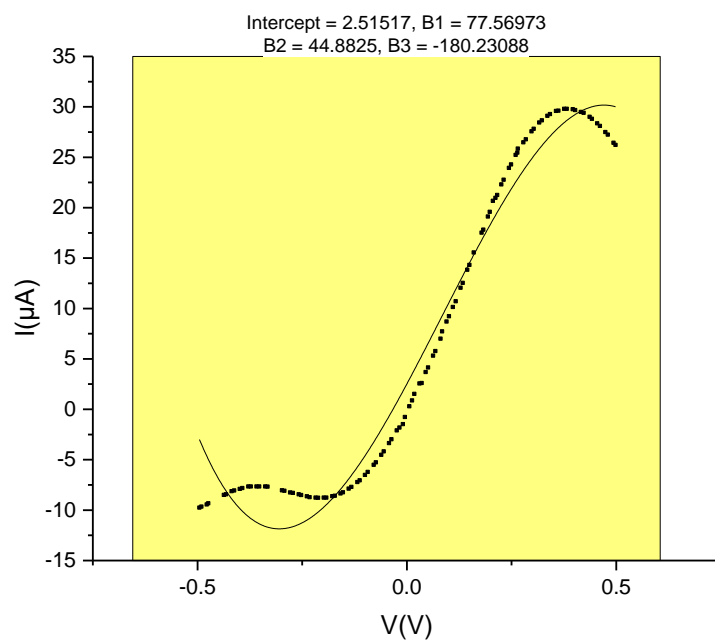


(a)

Figure A.3 Cu-MoS₂ current-voltage characteristic curves (a) linear fitting; (b) quadratic fitting; (c) cubic fitting (Continued).

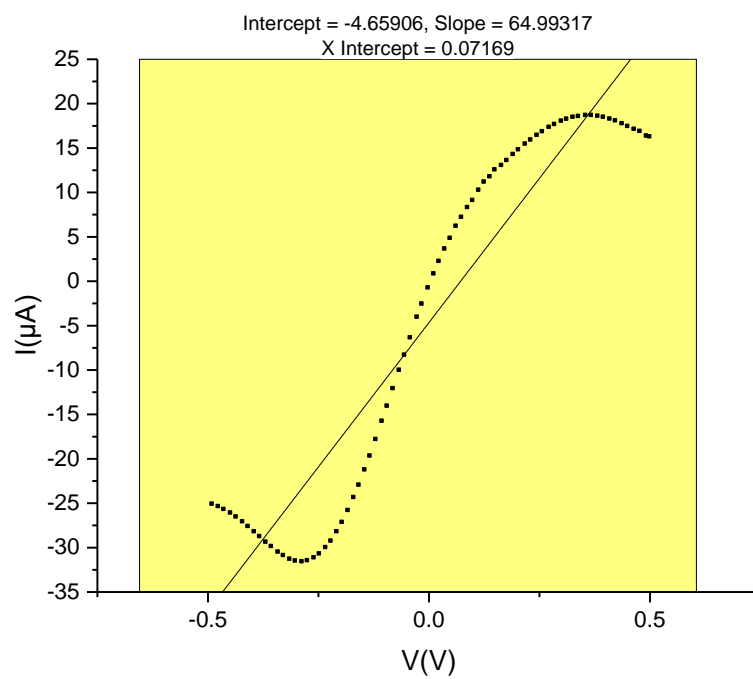


(b)

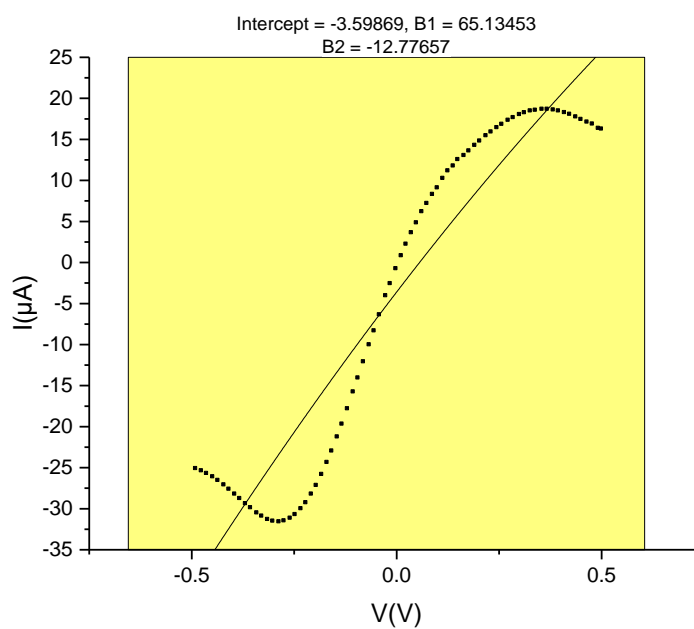


(c)

Figure A.3 (Continued) Cu-MoS₂ current-voltage characteristic curves (a) linear fitting; (b) quadratic fitting; (c) cubic fitting.

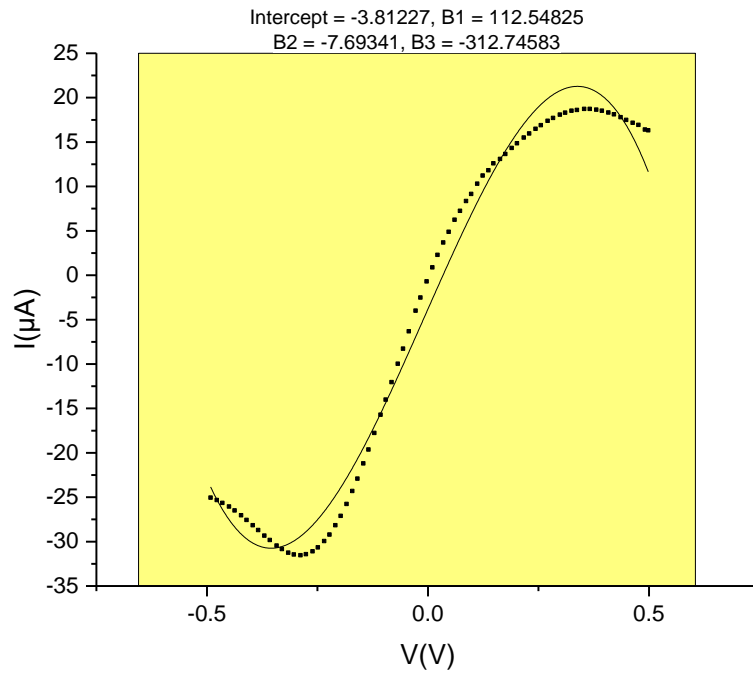


(a)



(b)

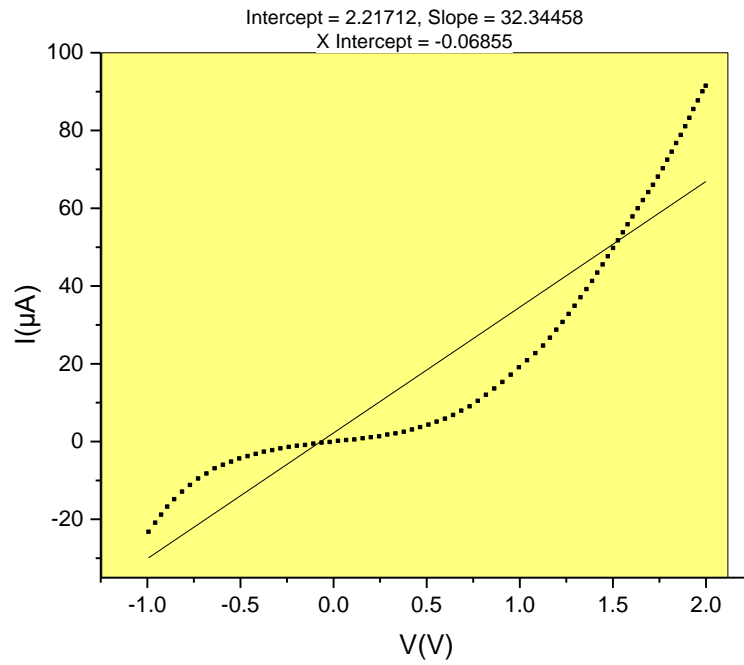
Figure A.4 Pt-MoS₂ current-voltage characteristic curves (a) linear fitting; (b) quadratic fitting; (c) cubic fitting (Continued).



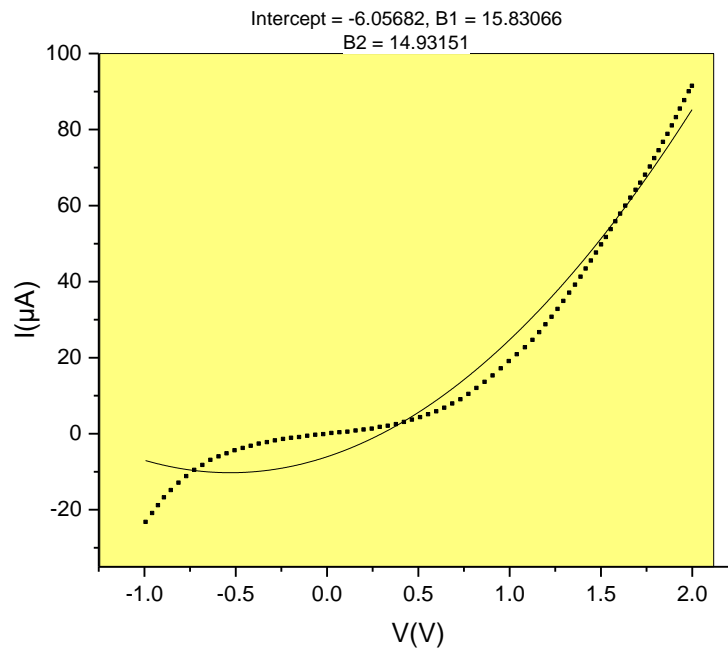
(c)

Figure A.4 (Continued) Pt-MoS₂ current-voltage characteristic curves (a) linear fitting; (b) quadratic fitting; (c) cubic fitting.

The following figures are the fitting results obtained from Figure 5.3. From these figures, we can confirm that the curves describe a strictly increasing function. It is different from the curves in Figure 5.2.

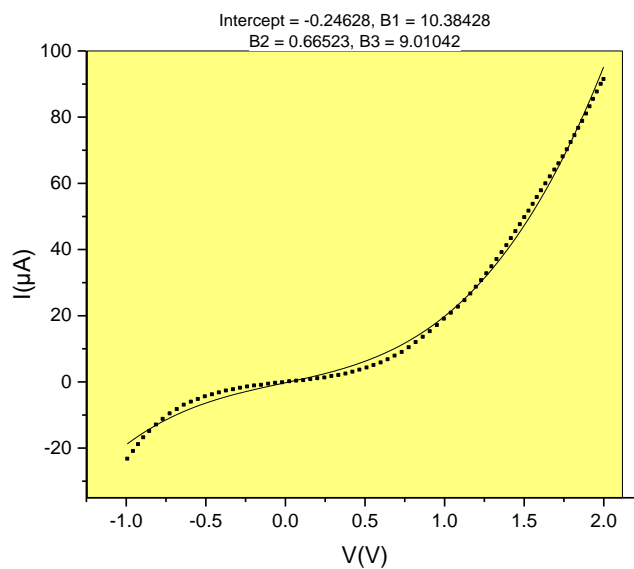


(a)



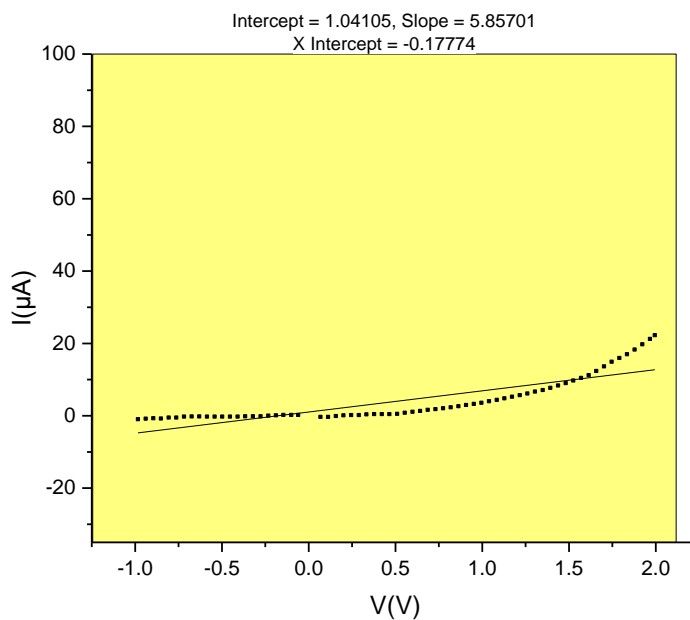
(b)

Figure A.5 Al-MoS₂ contact current-voltage characteristic curves (a) linear fitting; (b) quadratic fitting; (c) cubic fitting (Continued).



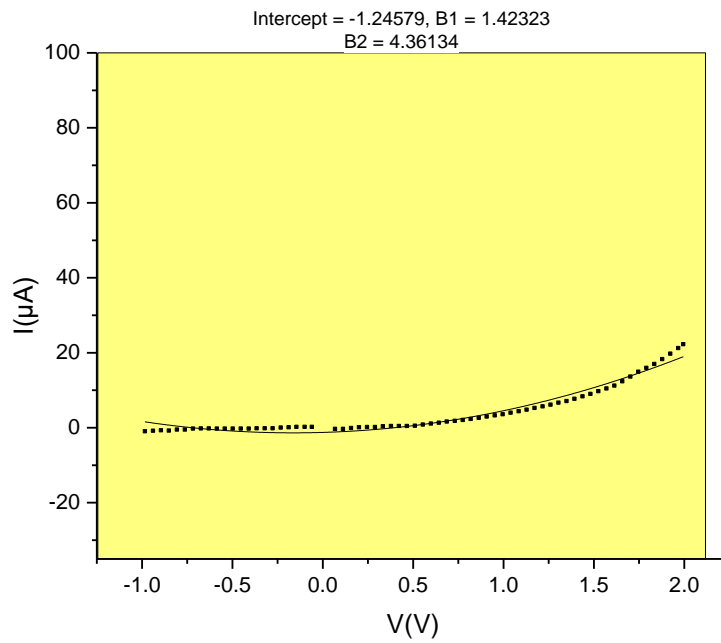
(c)

Figure A.5 (Continued) Al-MoS₂ contact current-voltage characteristic curves (a) linear fitting; (b) quadratic fitting; (c) cubic fitting.

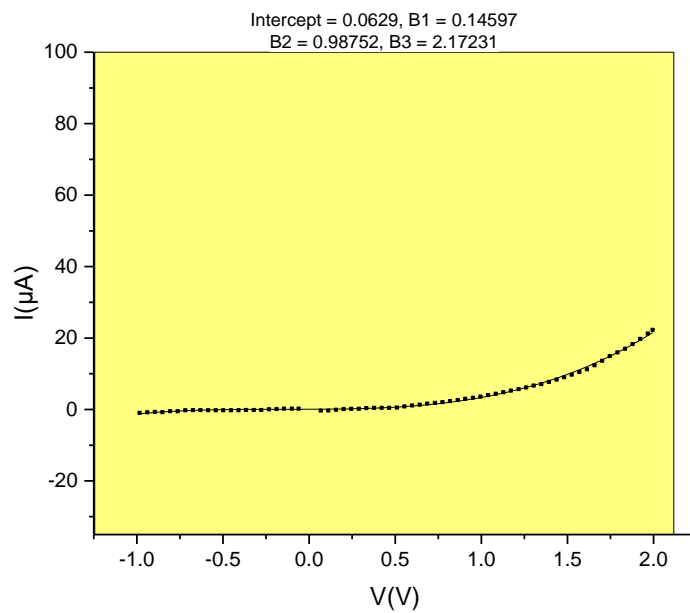


(a)

Figure A.6 Au-MoS₂ contact current-voltage characteristic curves (a) linear fitting; (b) quadratic fitting; (c) cubic fitting (Continued).

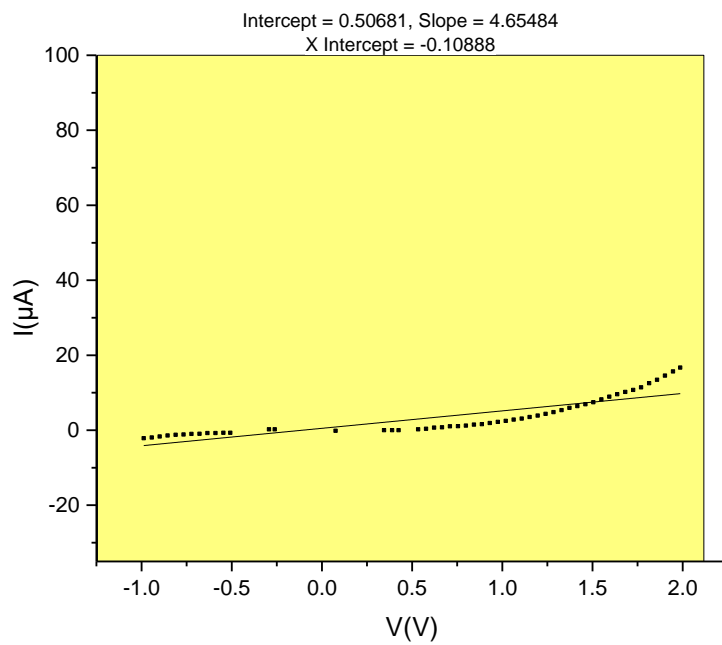


(b)

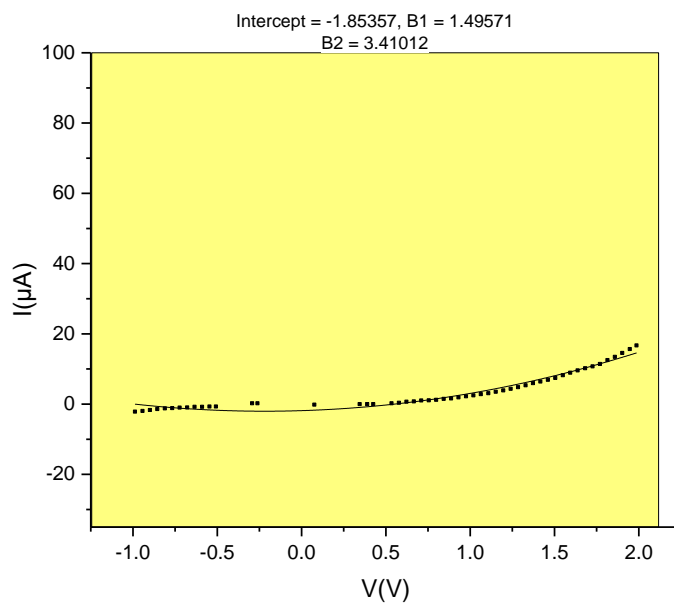


(c)

Figure A.6 (Continued) Au-MoS₂ contact current-voltage characteristic curves (a) linear fitting; (b) quadratic fitting; (c) cubic fitting.

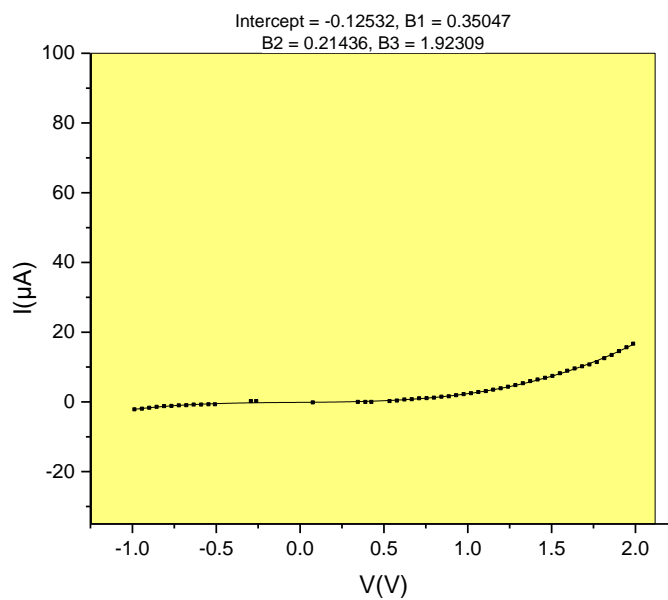


(a)



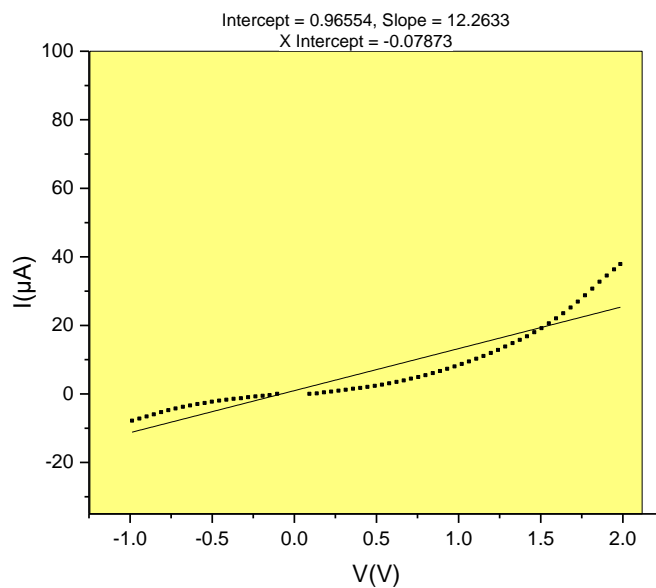
(b)

Figure A.7 Pt-MoS₂ contact current-voltage characteristic curves (a) linear fitting; (b) quadratic fitting; (c) cubic fitting (Continued).



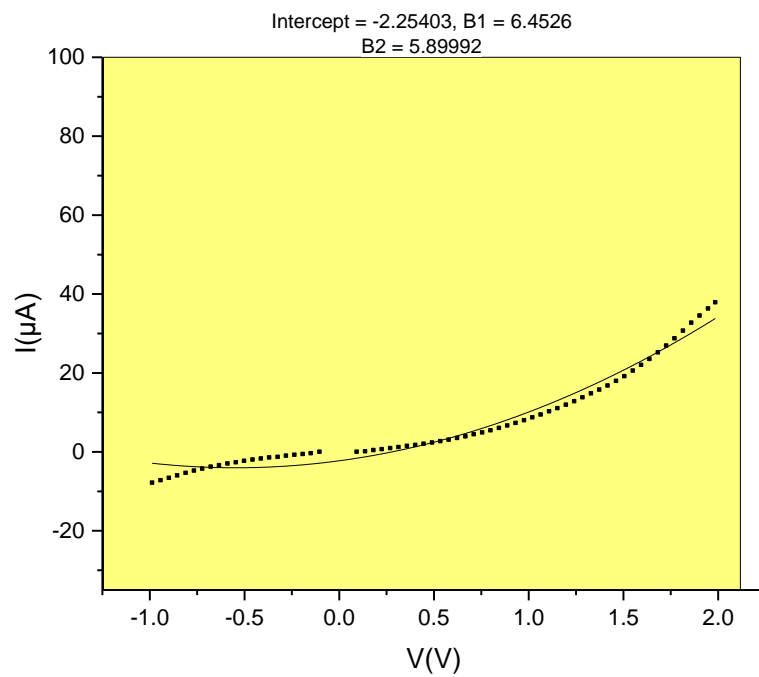
(c)

Figure A.7 (Continued) Pt-MoS₂ contact current-voltage characteristic curves (a) linear fitting; (b) quadratic fitting; (c) cubic fitting.

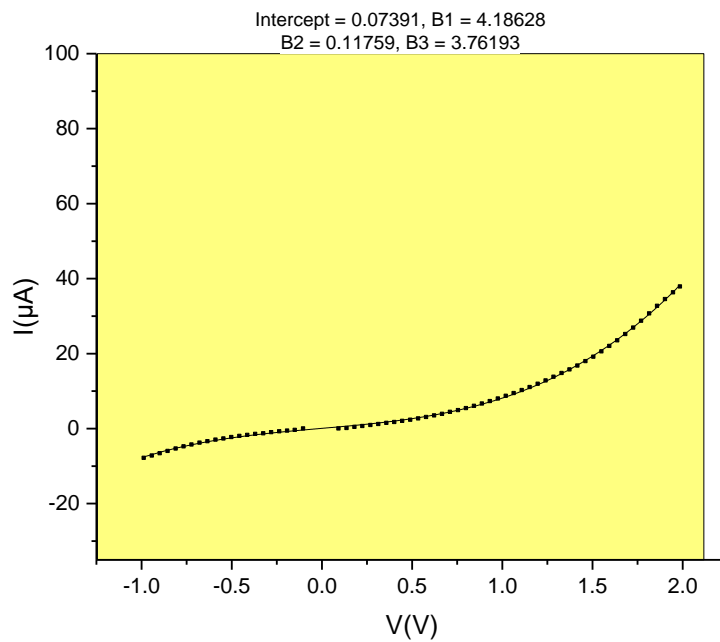


(a)

Figure A.8 W-MoS₂ contact current-voltage characteristic curves (a) linear fitting; (b) quadratic fitting; (c) cubic fitting (Continued).



(b)



(c)

Figure A.8 (Continued) W-MoS₂ contact current-voltage characteristic curves (a) linear fitting; (b) quadratic fitting; (c) cubic fitting.

REFERENCES

1. Lin, Z., et al., *2D materials advances: from large scale synthesis and controlled heterostructures to improved characterization techniques, defects and applications*. 2D Materials, 2016. **3**(4): p. 042001.
2. Cao, W., et al., *A Compact Current-Voltage Model for 2D Semiconductor Based Field-Effect Transistors Considering Interface Traps, Mobility Degradation, and Inefficient Doping Effect*. IEEE Transactions on Electron Devices, 2014. **61**(12): p. 4282-4290.
3. Xu, Y., et al., *Contacts between Two- and Three-Dimensional Materials: Ohmic, Schottky, and p-n Heterojunctions*. ACS Nano, 2016. **10**(5): p. 4895-919.
4. Leonard, F. and A.A. Talin, *Electrical contacts to one- and two-dimensional nanomaterials*. Nat Nanotechnol, 2011. **6**(12): p. 773-83.
5. Allain, A., et al., *Electrical contacts to two-dimensional semiconductors*. Nat Mater, 2015. **14**(12): p. 1195-205.
6. Liu, H., et al., *Phosphorene: an unexplored 2D semiconductor with a high hole mobility*. ACS Nano, 2014. **8**(4): p. 4033-41.
7. Liu, Y., H. Xiao, and W.A. Goddard, 3rd, *Schottky-Barrier-Free Contacts with Two-Dimensional Semiconductors by Surface-Engineered MXenes*. J Am Chem Soc, 2016. **138**(49): p. 15853-15856.
8. Yamamoto, M., et al., *Self-Limiting Oxides on WSe₂ as Controlled Surface Acceptors and Low-Resistance Hole Contacts*. Nano Lett, 2016. **16**(4): p. 2720-7.
9. Novoselov, K.S., et al., *Electric field effect in atomically thin carbon films*. Science, 2004. **306**(5696): p. 666-9.
10. Geim, A.K. and K.S. Novoselov, *The rise of graphene*. Nat Mater, 2007. **6**(3): p. 183-91.
11. Ravindra, N.M., K.S. Kumar, and V.K. Srivastava, *Temperature and voltage dependence of the barrier height in SnO₂/Si solar cells*. physica status solidi (a), 1982. **70**(2): p. 623-630.
12. Murphy, E.L. and R.H. Good, *Thermionic Emission, Field Emission, and the Transition Region*. Physical Review, 1956. **102**(6): p. 1464-1473.
13. Crowell, C.R., *The Richardson constant for thermionic emission in Schottky barrier diodes*. Solid-State Electronics, 1965. **8**(4): p. 395-399.
14. Bilkan, Ç., et al., *A comparison of electrical characteristics in Al/p-Si (MS) and Al/C₂₀H₁₂/p-Si (MPS) type diodes using current-voltage (I-V) and capacitance-voltage (C-V) measurements*. Materials Science in Semiconductor Processing, 2015. **32**: p. 137-144.
15. Higashiwaki, M., et al., *Temperature-dependent capacitance-voltage and current-voltage characteristics of Pt/Ga₂O₃ (001) Schottky barrier diodes fabricated on n-Ga₂O₃ drift layers grown by halide vapor phase epitaxy*. Applied Physics Letters, 2016. **108**(13): p. 133503.
16. Kumar, A., et al., *Electronic stability and electron transport properties of atomic wires anchored*

- on the MoS_2 monolayer. *Phys Chem Chem Phys*, 2014. **16**(37): p. 20157-63.
17. Luongo, G., et al., *I-V and C-V Characterization of a High-Responsivity Graphene/Silicon Photodiode with Embedded MOS Capacitor*. *Nanomaterials* (Basel), 2017. **7**(7).
 18. Rhoderick, E.H., *Metal-semiconductor contacts*. IEE Proceedings I Solid State and Electron Devices, 1982. **129**(1): p. 1.
 19. Kobayashi, K. and J. Yamauchi, *Electronic structure and scanning-tunneling-microscopy image of molybdenum dichalcogenide surfaces*. *Physical Review B*, 1995. **51**(23): p. 17085-17095.
 20. Schönfeld, B., J.J. Huang, and S.C. Moss, *Anisotropic mean-square displacements (MSD) in single-crystals of 2H- and 3R-MoS₂*. *Acta Crystallographica Section B Structural Science*, 1983. **39**(4): p. 404-407.
 21. Haynes, W.M., *CRC Handbook of Chemistry and Physics*. 97th Edition ed. 2016: CRC Press
 22. Wilson, J.A. and A.D. Yoffe, *The transition metal dichalcogenides discussion and interpretation of the observed optical, electrical and structural properties*. *Advances in Physics*, 1969. **18**(73): p. 193-335.
 23. Cheiwchanchamnangij, T. and W.R.L. Lambrecht, *Quasiparticle band structure calculation of monolayer, bilayer, and bulk MoS₂*. *Physical Review B*, 2012. **85**(20).
 24. van Schilfgaarde, M., T. Kotani, and S. Faleev, *Quasiparticle self-consistent GW theory*. *Phys Rev Lett*, 2006. **96**(22): p. 226402.
 25. van Schilfgaarde, M., T. Kotani, and S.V. Faleev, *Adequacy of approximations in GW theory*. *Physical Review B*, 2006. **74**(24).
 26. Kotani, T., M. van Schilfgaarde, and S.V. Faleev, *Quasiparticle self-consistent GW method: A basis for the independent-particle approximation*. *Physical Review B*, 2007. **76**(16).
 27. Li, T. and G. Galli, *Electronic Properties of MoS₂ Nanoparticles*. *The Journal of Physical Chemistry C*, 2007. **111**(44): p. 16192-16196.
 28. Lebègue, S. and O. Eriksson, *Electronic structure of two-dimensional crystals from ab initio theory*. *Physical Review B*, 2009. **79**(11).
 29. Jin, W., et al., *Direct measurement of the thickness-dependent electronic band structure of MoS₂ using angle-resolved photoemission spectroscopy*. *Phys Rev Lett*, 2013. **111**(10): p. 106801.
 30. Zeghbrock, B.V., *Principles of semiconductor devices*. 2004: Colorado University.
 31. O'Donnell, K.P. and X. Chen, *Temperature dependence of semiconductor band gaps*. *Applied Physics Letters*, 1991. **58**(25): p. 2924-2926.
 32. Tongay, S., et al., *Thermally driven crossover from indirect toward direct bandgap in 2D semiconductors: MoSe₂ versus MoS₂*. *Nano Lett*, 2012. **12**(11): p. 5576-80.
 33. Gołasa, K., et al., *Optical Properties of Molybdenum Disulfide (MoS₂)*. *Acta Physica Polonica A*, 2013. **124**(5): p. 849-851.
 34. Li, X. and H. Zhu, *Two-dimensional MoS₂: Properties, preparation, and applications*. *Journal of Materiomics*, 2015. **1**(1): p. 33-44.

35. Colthup, N., *Introduction to infrared and Raman spectroscopy*. 2012: Elsevier.
36. Long, D.A. and D. Long, *Raman spectroscopy*. Vol. 206. 1977: McGraw-Hill New York.
37. Xia, F., et al., *Two-dimensional material nanophotonics*. Nature Photonics, 2014. **8**(12): p. 899-907.
38. Gacem, K., et al., *High quality 2D crystals made by anodic bonding: a general technique for layered materials*. Nanotechnology, 2012. **23**(50): p. 505709.
39. Balendhran, S., et al., *Two-Dimensional Molybdenum Trioxide and Dichalcogenides*. Advanced Functional Materials, 2013. **23**(32): p. 3952-3970.
40. Wang, Q.H., et al., *Electronics and optoelectronics of two-dimensional transition metal dichalcogenides*. Nat Nanotechnol, 2012. **7**(11): p. 699-712.
41. Walia, S., et al., *Characterization of metal contacts for two-dimensional MoS₂ nanoflakes*. Applied Physics Letters, 2013. **103**(23): p. 232105.
42. Kaasbjerg, K., K.S. Thygesen, and K.W. Jacobsen, *Phonon-limited mobility in n-type single-layer MoS₂ from first principles*. Physical Review B, 2012. **85**(11).